Christoph Rohringer, BSc

Improvement of sorption thermal energy storage systems with the charge boost technology

Master's thesis

to achieve the degree of a

"Diplom-Ingenieur"

in

Process Engineering

Submitted at the

Graz University of Technology

Advisor:

Ao.Univ.-Prof.i.R. Dipl.-Ing. Dr.techn. Hans Schnitzer

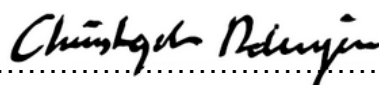Institute of Process and Particle Engineering

Dr. Georg Engel

AEE Intec

Graz, September 2016

STATUTORY DECLARATION

I declare that I have authored this thesis independently, that I have used no other than the declared sources-/resources, and that I have explicitly marked all material which has been quoted either literally or by content from the used sources.

Graz, 10th of October 2016 ....

Christoph Rohringer, BSc

EIDESSTATTLICHE ERKLÄRUNG

Ich erkläre an Eides statt, dass ich die vorliegende Arbeit selbstständig verfasst, andere als die angegebenen Quellen/Hilfsmittel nicht benutzt, und die den benutzten Quellen wörtlich und inhaltlich entnommenen Stellen als solche kenntlich gemacht habe. Das in TUGRAZonline hochgeladene Textdokument ist mit der vorliegenden Masterarbeit identisch.

Graz, am 10. Oktober 2016 ....

Christoph Rohringer, BSc

Acknowledgements

I would like to thank Hans Schnitzer and Georg Engel for their excellent supervision over the writing process of my thesis. Georg Engel always introduced me to new perspectives and ideas during our conversations and never failed to help me out when I encountered a problem.

Thanking the employees of AEE Intec cannot go without mentioning the measurement technology team in particular. Waldemar Wagner, although hunted by many Master students, always found the time to deal with the various problems that arose in the laboratory. Without Reinhard Pertschy, the automatic process control system would not exist and I would also be short of several technical insights. Last but not least, I want to thank Jakob Stranzl. Not only did he make the reconstruction of the testing plant possible in the first place, but he also turned it into an enjoyable experience.

Regarding not only this thesis but all of my studies up until this point, I want to thank Bernhard Maunz and Tobias Thaler. They have not only been great study companions and colleagues over the past five years, but also true friends.

I also want to thank my family who not only provided me with the possibility to dedicate myself to my studies in the first place, but who also always supported me and helped me out wherever they could. Special thanks go to my girlfriend Bettina Resch, who often reminded me that the world does not only revolve around numbers and tables.

Abstract

In this Master's thesis, a new concept for compact thermal energy storages is developed and tested via experiments. In order to do that, a new theoretical concept is implemented in existing sorption thermal energy storage systems, the so-called "charge boost technology". The main benefit of this approach is that it can reach a defined state of charge for sorption thermal energy storages at lower temperature levels than classic pure desorption processes. This makes it an interesting candidate for a number of applications in thermal energy storage technology.

As a first step, experiments are conducted to provide proof of principle concerning this theoretical concept. The results show that the charge boost technology does function as predicted and is indeed a viable option for further improvement of sorption thermal energy storages.

In a second step, a new process concept is developed by the author with strong focus on the utilization of the advantages the charge boost technology has over conventional desorption processes. This specification results in the development of a system which uses the charge boost technology to recharge an already discharged sorption thermal energy storage in winter. In addition to new process parameters, a material screening is performed as the charge boost technology enables the system to operate in a different temperature range than standard zeolite based systems. The material screening shows that silica gels may be suited better in the recharge unit whereas zeolite is still the better candidate for the main storage material. After the final design of the theoretical concept, the theoretical assumptions are tested via experiments.

Kurzfassung

Im Zuge dieser Masterarbeit wird ein neues Konzept für kompakte thermische Speicher entwickelt und mittels Experimenten getestet. Das theoretische Konzept des „Umladens" wird dabei in existierende Sorptionswärmespeicher implementiert. Der hauptsächliche Vorteil dieses neuen Konzepts ist das erreichen definierter Ladungszustände unter Verwendung niedrigerer Temperaturen als bei der klassischen Desorption ohne Umladen. Dieser Umstand prädestiniert das Konzept für den Einsatz in einer Vielfalt von Anwendungsmöglichkeiten im Bereich der thermischen Sorptionswärmespeicher.

In einem ersten Schritt werden Experimente durchgeführt um das bis dato rein theoretische Prinzip praktisch zu validieren. The Ergebnisse zeigen, dass der Umladeprozess entsprechend der Theorie in der Realität umgesetzt werden kann. Das macht diese Technologie zu einer vielversprechenden Option für die Verbesserung der Eigenschaften von thermischen Sorptionswärmespeichern.

Im zweiten Abschnitt dieser Arbeit wird eine neue Prozessführung entwickelt, die speziell dafür konzipiert wurde um die Vorteile des Umladeprinzips optimal zu nutzen. Ein System wird definiert, in dem der Umladeprozess verwendet wird um bereits entladene Speichereinheiten während der Wintermonate nachzuladen. Zusätzlich zu der Definition neuer System- und Prozessparameter wird eine Materialstudie durchgeführt um festzustellen ob sich andere Sorptionsmaterialen für den neuen Temperaturbereich besser eigenen als das standardmäßig eingesetzte Zeolith. Die Materialstudie zeigt, dass Silikagele voraussichtlich besser für eine Verwendung in der Umladeeinheit geeignet sind während Zeolith als Hauptspeicher-Material bessere Eigenschaften aufweist. Nachdem das finale Design für die neue Prozessführung abgeschlossen ist, wird diese mittels Experimenten getestet.

List of symbols

Symbol	Unit	Description
A	-	Antoine parameter for water
A_x	$\frac{kJ}{kg}$	adsorption potential
B	°C	Antoine parameter for water
C	°C	Antoine parameter for water
c_{p_ads}	$\frac{kJ}{kgK}$	specific heat capacity of the adsorbent
c_{p_coll}	$\frac{J}{m^2K}$	specific heat capacity of collector
c_{p_water}	$\frac{kJ}{kgK}$	specific heat capacity of water
E	$\frac{J}{g}$	characteristic free energy of adsorption
F_c	-	cycle efficiency factor
K	-	equilibrium constant
L_R	$\frac{mbar*l}{s}$	leakage rate
M	$\frac{g}{mol}$	molar mass
m	kg	mass
Δm	kg	change in mass
m_{ads}	kg	mass of adsorbed water
m_{MS}	kg	mass main storage temperature
m_{REC}	kg	mass recharge unit
n	-	exponent for the Dubinin-Astakhov equation
p	mbar	pressure
Δp	mbar	pressure gradient
p_S	mbar	saturation vapour pressure
$P_{aux,charge}$	kJ	auxiliary energy for the charge process
$P_{aux,discharge}$	kJ	auxiliary energy for the discharge process
Q	kJ	energy
Q_{ads}	$\frac{Wh}{kg_{material}}$	maximal adsorption energy per kg of material
$Q_{ads40\,°C}$	$\frac{Wh}{kg_{material}}$	maximal adsorption energy per kg of material for a desorption temperature of 40 °C
Q_{charge}	kJ	thermal energy used to charge a storage system

$Q_{discharge}$	kJ	discharged thermal energy from a storage system
Q_{solar_daily}	Wh	total solar radiation energy available during one day
Q_{solar_winter}	Wh	total amount of solar radiation energy available during winter
Q_{stored}	Wh	total amount of stored thermal energy
R	$\frac{kJ}{kgK}$	ideal gas constant
$R[\Omega]$	Ω	electrical resistance
T	°C	temperature
ΔT	°C	temperature gradient
V	m³	volume
v	m³	adsorption volume
W	m³	currently available pore volume
W_0	m³	total available pore volume
X	%	moisture load
ΔX	%	change in moisture load
X_{max}	%	maximal moisture load
ΔX_{max}	%	maximum possible change in moisture load
$\Delta X_{40\,°C}$	%	maximum possible change in moisture load for a desorption temperature of 40 °C
X_{start}	%	moisture load at the start of the process
X_{end}	%	moisture load at the end of the process

α_1	$\frac{W}{m^2K}$	linear heat loss coefficient of collector
α_2	$\frac{W}{m^2K^2}$	quadratic heat loss coefficient of collector
δ^*	$\frac{kg}{m^3}$	Polanyi density
η_0	-	optical efficiency of collector
η_{cycle}	-	cycle efficiency
η_{system}	-	system efficiency
θ	%	coverage rate
ρ	$\frac{kg}{m^3}$	density
ρ_0	$\frac{kg}{m^3}$	reference density of water at 20 °C

Table of contents

1   Introduction

1.1 Motivation for this work

The upcoming shortage of fossil fuels as well as the already occurring climate change lead to a growing interest in the usage of renewable energies [1], [2], [3], [4], [5], [6]. The main problem with energy sources like solar energy is the discrepancy between supply and demand which occurs in two ways [7], [8]. Firstly, the majority of the radiation is received during the day when the sun provides its energy to the collector. However, the peak in energy demand usually occurs in the evening. Although this is problematic, it is not the main issue of solar energy. The greatest obstacle to overcome is the gap between summer and winter. In summer, when solar energy is abundant, no space heating is needed. During the heating period in winter when heat is very much required, the lowered solar radiation cannot supply enough energy to cover that demand as depicted in Figure 1-1 [9].
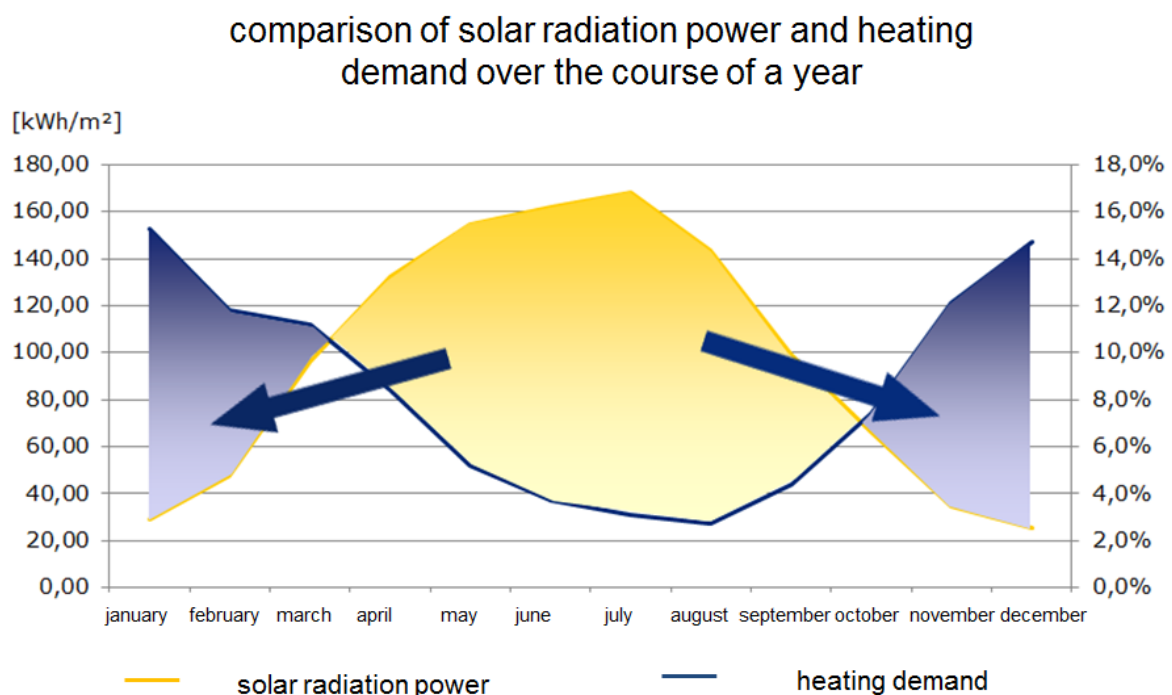

Figure 1-1: Comparison of solar radiation power and heating demand over the course of a year [9].

This means that the currently biggest challenge for solar energy implementation in housing is the long term storage of the excess energy in summer for the use during the high energy demand periods in winter [10].

Additionally, research is strongly leaning towards the development of compact storage possibilities as more required space reduces the cost effectiveness of the system. The goal of this thesis is to develop such a compact thermal energy storage system by integrating a newly found concept, the so-called "charge boost" technology into an already existing storage system design. In the following chapters, the necessary basics of thermal energy storage as well as the theoretical concept of the charge boost technology will be explained in detail.

1.2 Types of storage methods

The storage of thermal energy has been a major topic of many research projects throughout the past years [11]. Therefore, many different approaches exist. The main categories of thermal energy storages are distinguished by their type of energy storage principle. There are three main forms of thermal energy storages [12]:

- Sensible heat
  Sensible heat is stored as a temperature difference of a material times its heat capacity. The sensible heat storage material is naturally hotter than its surrounding, which means that heat loss is inevitable and can only be reduced (insulation), but not completely avoided.

- Latent heat
  Latent heat is stored as a phase change potential. Most commonly, the change of state from liquid to solid is used, resulting in a smaller difference of temperature necessary to store the same amount of energy as in a sensible storage.

- Thermo-chemical heat
  Also, reversible chemical or physical reactions can be used for heat storage. They have the same benefits as latent heat storages and are able to adjust their charge and discharge temperatures to the needs of the process. Especially ab- and adsorption processes are used in state of the art storages. As the main focus of this Master's thesis is (ad)sorption thermal energy storage, the following chapter will give a quick overview of the adsorption process and the existing theoretical models.

2 Theory of Adsorption

2.1 General information

Adsorption stands for a physical phenomenon where a bulk substance, usually a gas or liquid, is bound to the surface of another substance (liquids or most commonly solids). This is usually an exothermal process [13]. The molecules of the gas phase, the so-called adsorbate, start to form layers at the interface with the adsorbent. Equilibrium is reached when ad- and desorption rate are equal which results in constant pressure in the gas phase and a constant amount of adsorbed gas molecules on the adsorbent surface (see Figure 2-1).
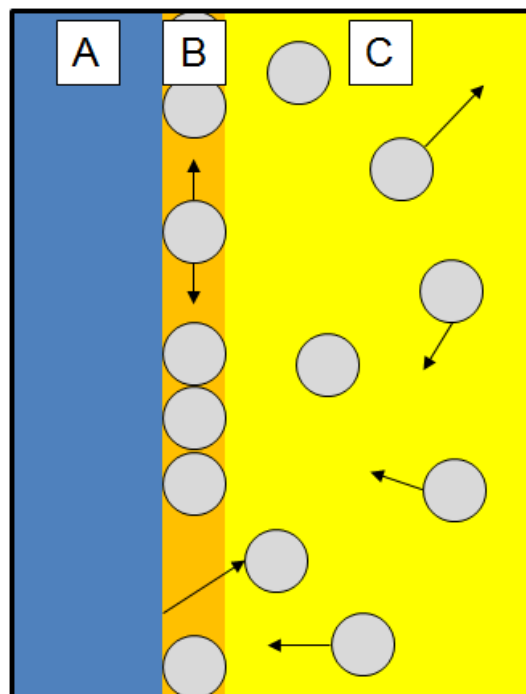
Figure 2-1: Schematic of the adsorption process. (A) adsorbent surface, (B) boundary layer with adsorbed gas molecules (grey circles), (C) adsorbate phase with free gas molecules.

In this master's thesis the adsorbate is pure water vapour (steam) and the adsorbent is solid substance which will be defined for the respective systems later on. Different approaches exist to describe adsorption processes mathematically. The desired outcome of these theories is to obtain a formula that describes the adsorption equilibrium in dependency of the physical properties of the system, namely pressure, temperature and moisture load. A selection of the most common methods is presented in the following chapters, sorted by increasing complexity.

2.2 Langmuir

The adsorption model of Langmuir is the simplest model with an approach that builds upon a physical interpretation of the adsorption process [14]. Langmuir imposes three conditions for his model:

- Adsorption can only build up a monolayer of molecules at the boundary layer.

- The enthalpy of adsorption is the same for all molecules and does not depend on the number of adsorbed molecules.

- The adsorbed molecules do not influence each other.

The theory of Langmuir follows the law

$$\theta = \frac{K * p}{1 + K * p} \tag{2.1}$$

It states a correlation between the coverage rate θ of the solid and the equilibrium pressure p. The coverage rate itself is the ratio between occupied spaces and available spaces on the surface of the adsorbent. K is the equilibrium constant and a thermo-physical property of the adsorbate-adsorbent pair. This mathematical formula can reach two limit cases. If the pressure approaches zero, the formula becomes

$$\theta = \frac{K * 0}{1 + K * 0} = \frac{0}{1} = 0 \tag{2.2}$$

and the coverage rate approaches zero. On the other hand, if the pressure increases to infinity, the formula can be written as

$$\theta = \frac{K * \infty}{1 + K * \infty} = \frac{\infty}{\infty} = 1 \tag{2.3}$$

with a coverage rate of 1. The behaviour of real systems can vary within those two boundaries. However, this approach is very simple and cannot depict the adsorption behaviour of real systems with sufficient accuracy over wide ranges of θ. In fact, it is only valid at low pressures, due to Langmuir's definition that the bulk gas phase behaves like an ideal gas.

2.3 Theory of Polanyi

Polanyi [15] categorizes the forces occurring during adsorption. They can be divided into three types:

- Electrostatic forces

- Valence forces

- Dispersion forces

He also states that the different forces that affect a molecule near the surface of an adsorbent can be summarized as so-called adsorption potential. The adsorption process is then described as an interaction between the molecule and this potential. The result of Polanyi's derivations is equation 2.4:

$$A_x = RT * \ln\left(\frac{p_S}{p}\right)$$

(2.4)

Furthermore, the adsorbed gas is treated like a liquid phase, which means that the pressure p_S is the saturation pressure of the liquefied gas phase at system temperature. In order to describe its behaviour, a density δ^* is introduced which connects the mass of adsorbed water m_{ads} to the adsorption volume v:

$$v = \frac{m_{ads}}{\delta^*}$$

(2.5)

As the adsorption potential A_x is not temperature dependent, equations 2.4 and 2.5 can be used to describe the adsorption behaviour of a substance pair for the whole temperature range [16].

2.4 Theory of Dubinin

Dubinin extends the theory of Polanyi [17], [18], [19]. He states that, for very small pores, the effect of volume filling is dominating over the surface coverage. He also states that the properties of the liquid on the adsorbent can differ from those of a free liquid. In order to describe the process of volume filling along with this adapted liquid behaviour, he introduces equation 2.6.

$$X_{max} = \rho(T) * W_0 \tag{2.6}$$

W_0 represents the total available pore volume of the adsorbent. Multiplied with the temperature dependent density of the condensed adsorbate $\rho(T)$ it results in the maximum moisture load of the system X_{max}. In the same manner, the current moisture load can be expressed using the current amount of occupied pore volume (see equation 2.7).

$$X = \rho(T) * W \tag{2.7}$$

By plotting the adsorption potential A_x as a function of the adsorption volume W, the so-called "characteristic curve" can be obtained. This correlation contains the information of all adsorption isotherms below the critical temperature for a given adsorbate-adsorbent pair. The respective formula is depicted in equation 2.8.

$$W = W(A_x) = W\left(RT * ln\left(\frac{p_S}{p}\right)\right) \tag{2.8}$$

The complete derivation for this equation can be found in Hauer [13] as well as Bering et al. [18] but is not carried out here. In order to mathematically solve this formula, different approaches have been made.

2.4.1 Dubinin-Radushkevich

Dubinin and Radushkevich postulated an empirical approach to solve the original problem [20], [21]. The result is stated in equation 2.9.

$$W = W_0 * exp\left[\left(-\frac{RT}{E} * ln\left(\frac{p_S}{p}\right)\right)^2\right] \tag{2.9}$$

The newly introduced variable E represents the characteristic free energy and is specific for each adsorbate-adsorbent pair. By using equation 2.6 and multiplying equation 2.9 with the temperature dependent density $\rho(T)$, the desired function (see chapter 2.1), which connects pressure, temperature and moisture load, can be obtained (equation 2.10).

$$X = X_{max} * exp\left[\left(-\frac{RT}{EM} * ln\left(\frac{p_S}{p}\right)\right)^2\right] \tag{2.10}$$

The molar mass M in the fraction is needed to adjust the ideal gas constant to the specific gas constant of water (adsorbate phase).

2.4.2 Dubinin-Astakhov

Dubinin and Astakhov further refined this model [22]. They no longer demand 2 as fixed value for the exponent but rather suggest that the variable should be varied for each adsorbate-adsorbent pair. It usually varies between 1 and 3 for most systems [13]. The resulting equation is

$$X = X_{max} * exp\left[\left(-\frac{RT}{EM} * ln\left(\frac{p_S}{p}\right)\right)^n\right]$$

(2.11)

or rewritten for the pressure p

$$p = p_S * exp\left[\frac{EM}{RT} * \left(ln\left(\frac{X}{X_{max}}\right)\right)^{\frac{1}{n}}\right]$$

(2.12)

This equation contains the material specific parameters p_S, M, E, n and X_{max} as well as the system variables p and T. X_{max} further consists of $\rho(T) * W_0$ (see equation 2.6). The saturation vapour pressure p_S can be calculated with a simple Antoine equation with sufficient accuracy (parameters see appendix, Antoine equation see [23]). For the temperature dependent density of water $\rho(T)$, the empirical formula 2.13 is used as in the COMTES project [24], [25]:

$$\rho(T) = \frac{\rho_0}{(1 + 0,00021 * (T(°C) - 20))}$$

(2.13)

ρ_0 represents the reference density of water at 20 °C. The other material specific values however, have to be determined via literature research (M) or experiments (E, n, W_0) and are given for every considered system in the appendix. Equations 2.11 and 2.12 are the main tools for calculation throughout this work.

2.5 Usage of isosteric curves to depict sorption processes

The different mathematical models described in the previous chapters can be used to calculate adsorption phenomena. Since, in this Master's thesis, different combinations of heating, cooling, adsorption and desorption are described, the so-called isosteric diagram is introduced at this point. The different mathematical models enable the calculation of a function $F = F(T, p, X) = 0$. With this function, the correlation of temperature, pressure and moisture content can be described. It is therefore possible to depict each point of state for the adsorbent/steam system in the isosteric diagram. As it is a three dimensional problem, several curves have to be used to plot the system in a two axes figure. Usually, the ordinate axis represents pressure while the abscissa depicts the temperature. Therefore, the third variable, the moisture content, is plotted as a set of curves. Figure 2-2 shows such an isosteric diagram for the adsorbate-adsorbent pair water-zeolite 13XBF, calculated by Mette for the COMTES project [24], [25] using the Dubinin-Astakhov approach.
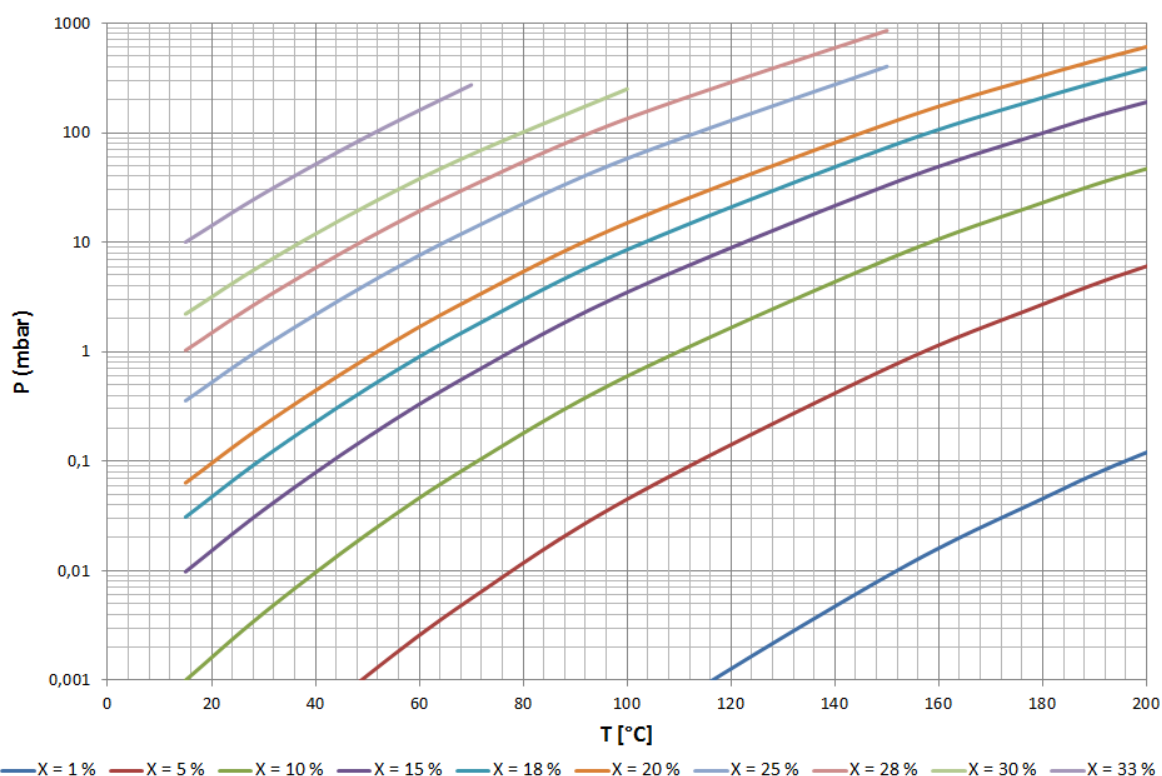

Figure 2-2: Isosteric diagram for the material pair water-zeolite 13XBF calculated by Mette [24], [25].

As stated before, the different curves show the system behaviour for different moisture contents. The boundary value is the maximum load of the adsorbent and equals the vapour pressure curve of water (topmost curve in Figure 2-1Figure 2-2). In order to understand the discussions in the following chapter better, the different ideal changes of state are described in Figure 2-3.
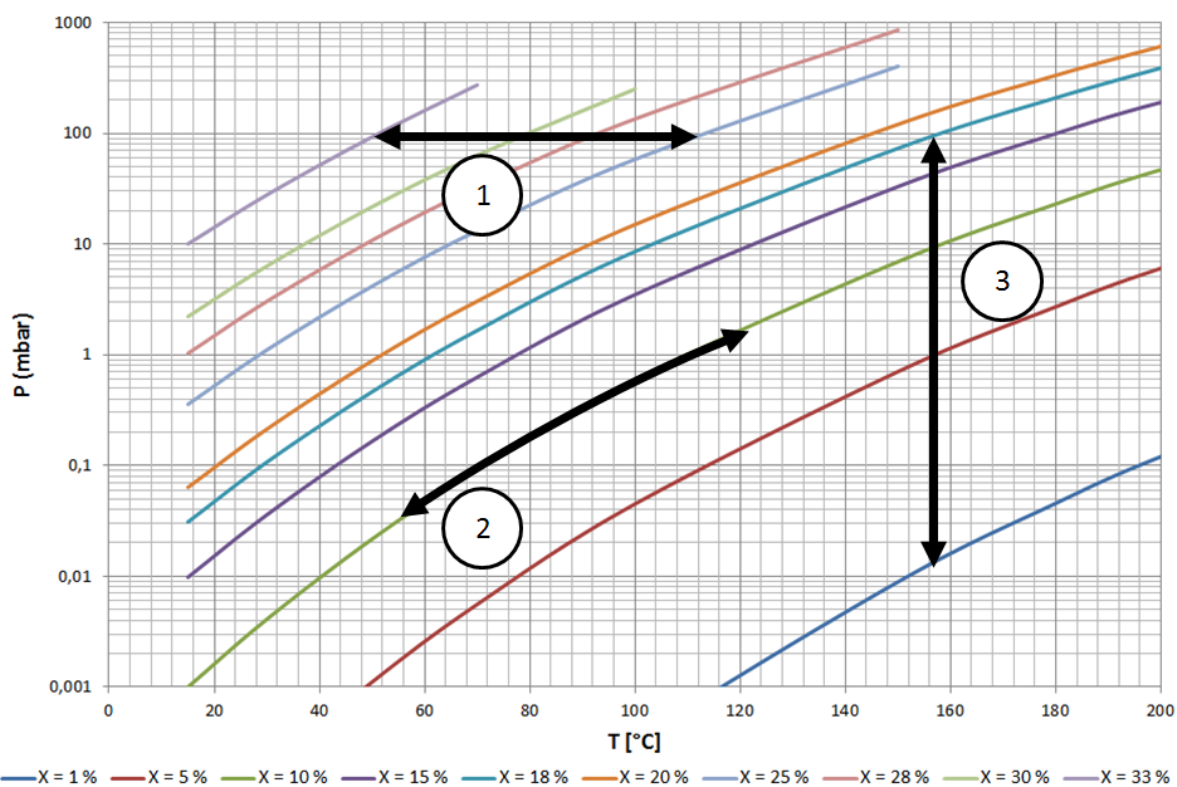

Figure 2-3: Changes of state in an adsorption system. **1)** Isobaric heating or cooling, **2)** Isosteric heating or cooling, **3)** Isothermal increase or decrease in pressure, with a change in moisture load.

3 Sorption energy storage systems

3.1 General setup of a typical sorption energy storage system

In this chapter the general setup for a sorption energy system is described.

As stated in the previous chapter, adsorption is always an exothermal process. This means that a dry adsorbent holds a thermo-physical potential to release energy in the form of heat as soon as it comes in contact with water. This effect can be used to store thermal energy as depicted in Figure 3-1.
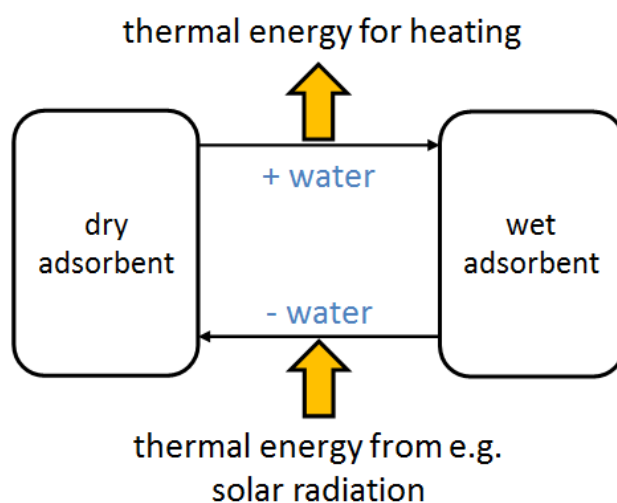

Figure 3-1: Schematic of an adsorption/desorption cycle with the respective energy streams.

The thermal energy depicted in Figure 3-1 can be stored and released at different temperature levels as well, enabling the system to operate like an adsorption heat pump [26]. However, a sorption energy storage system exceeds the adsorption heat pump as it can operate with a time delay between the charge and discharge step. As the adsorbent has ambient temperature when not used, the thermal energy can be stored with virtually no losses for long periods of time. This predestines the adsorption energy storage system for long term storage applications. Regarding the storage of thermal energy acquired during the summer for the winter period, an adsorption energy storage system exceeds the performance of a sensible hot water tank. The system is dried via solar radiation during the summer months. As soon as heating demand arises, the adsorbent is brought in contact with water (in the form of steam) and releases the stored energy at the desired temperature level.

After discussing the theoretical principle underlying sorption energy storage systems, a real life setup for such an apparatus is described in the following paragraphs. At the baseline, there are two main categories of sorption energy storage systems [27].

- Closed systems

- Open systems

As the name suggests, closed systems are completely isolated from the environment considering mass transport. They only experience heat transfer through the system borders. Open systems, on the other hand, use a feed medium which is discharged after the process is finished, often times in a continuous way. Most commonly air is used as a working medium. As the focus of this master's thesis solely concerns closed systems, only the basic setup for those instalments will be discussed.

A closed sorption energy storage system (CSESS) essentially consists of two main parts. These two components are the **water storage**[1] and the **zeolite storage**. The two units need to be separated spatially in order to avoid a sorption reaction during the storage period and a thereby caused heat loss (see Figure 3-2).
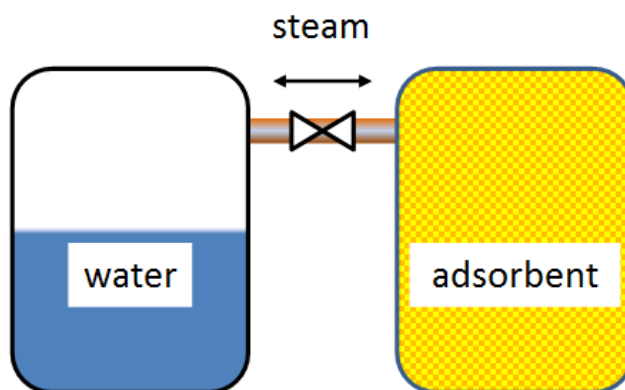
Figure 3-2: Simplified schematic of a CSESS.

---

[1] For the CSESS investigated at AEE Intec, the water storage also operates as the evaporating and condensing unit.

Closed systems usually operate under vacuum, which means that only steam is present as gas phase. Furthermore, the pressure level inside the system is determined by the temperature of the water phase (the saturation vapour pressure for the given temperature). In order to generate or move steam in the system, energy is required. Depending on which time of the year the operation takes place, these energies can originate from different sources (Table 3-1). Generally speaking, the two main groups are **high temperature energy** and **low temperature energy**. In addition to the heat sources, also heat sinks are a necessity for the system in order for it to function.

Table 3-1: Different heat sources for both low and high temperature levels as well as possible heat sinks for CSESS.

Low temperature heat source	High temperature heat source	Heat sink
Ground heat collector	Solar radiation	Ground heat collector
Buffer storage	Electricity	Ice storage
Air	-	Air

In this master's thesis, only CSESS are investigated which operate with solar radiation as high temperature energy source. These systems are charged[2] during the summer period and discharged during the heating period in winter when solar radiation alone is no longer sufficient for space heating. The required low temperature energy source for evaporating the water content is provided by a ground heat collector which can supply constant power throughout the winter period and is unaffected by changes of the weather conditions. The ground heat collector also operates as heat sink for the discharge of the condensation energy during summer. Figure 3-3 shows the process in the isosteric diagram.
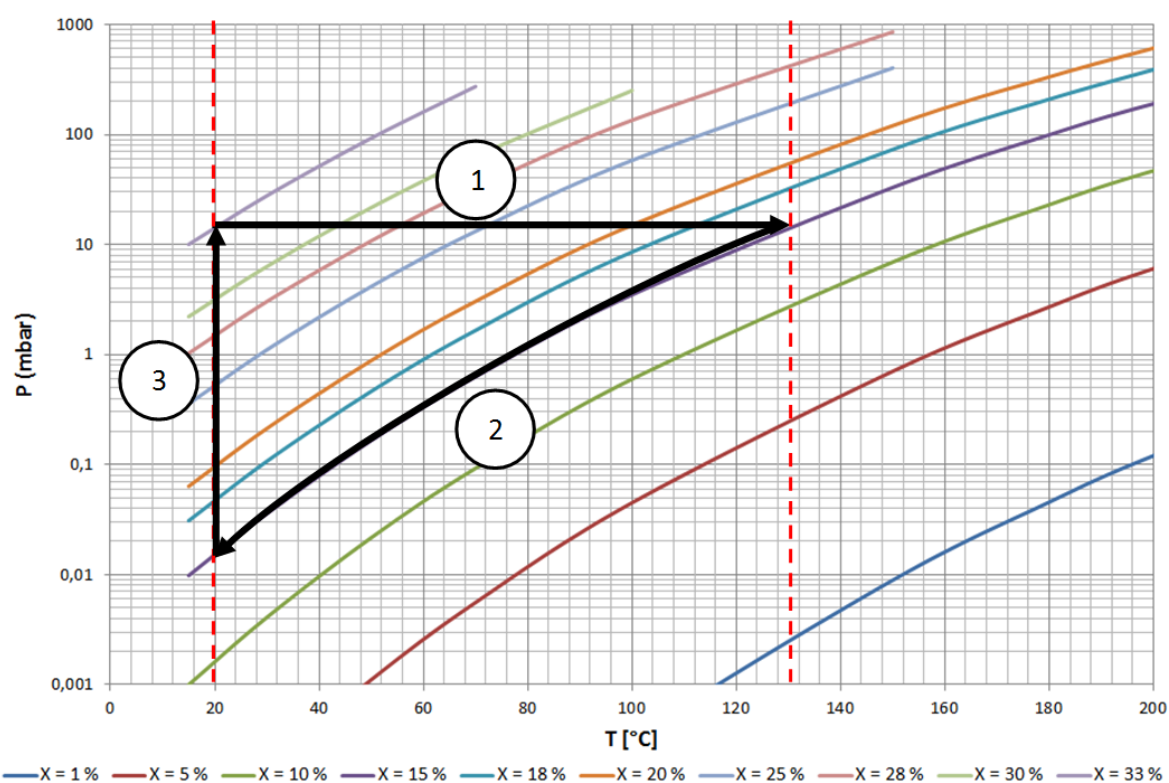
Figure 3-3: Charging process for a classic CSESS. **1)** Isobaric heating during the summer months, reducing the moisture content of the adsorbent at constant pressure. **2)** Isosteric cooling of the unit when the heating is stopped, going into storage mode. **3)** Isothermal heating as soon as thermal energy is required. The temperature at which this process is carried out depends on the desired temperature level of the discharged heat. In this example it is at 20 °C in order to provide a clearly arranged figure to the reader.

---

[2] In order to clarify the terminology, charging always means the increase of stored energy, hence the discharge of water from the adsorbent (increasing its thermo-chemical potential). On the other hand, discharging stands for the removal of stored energy from the system, resulting in an increase of the water content in the adsorbent.

The process can store more energy if the available pressure and moisture load gradient for step three is larger. This means that the efficiency is limited by the two system temperatures, the low temperature level of the heat sink and the high temperature level of the thermal energy provided by solar radiation. In order to store more energy within the system, either the heat sink temperature has to be decreased or the high temperature level has to be increased. However, both of these two possibilities have disadvantages as well. Lowering the heat sink temperature artificially compared to a ground heat sink results in a cooling demand which, in return, creates and additional energy demand and is therefore not viable. Also, increasing the high temperature level is problematic as solar thermal collectors have a lower efficiency at high temperatures [28].

In the works of Mette et al. [29] and subsequently Müller [30] a new mode of operation is suggested which would further improve the energy storage capabilities and reduce the material requirements of the system without the need for a change of the system temperatures. This so-called "charge boost" technology is explained in the following chapter.

3.2 Charge boost technology

The charge boost technology uses the effect that a vessel filled with adsorbent reduces its pressure if it is cooled down in an isosteric way (compare with 2 in Figure 3-3). When integrating two sorption vessels in a system, the cooled one can be connected to the hot one and steam will be transported from higher to lower pressure. This way the SOC[3] of the hot storage is increased further, whereas the one of the colder storage is decreased.

As suggested by Müller [30], the system is designed with a smaller "recharge unit" and a bigger "main storage unit". The reason for the recharge unit being smaller is that it should be possible to completely regenerate the used recharge unit during one day using solar radiation energy. By using this setup, the bigger main storage unit can be charged using the smaller recharge unit in addition to direct desorption of both units. The routine for the charge boost process is described in Figure 3-4.

---

[3] SOC = State of charge, a percentage value calculated by the ratio of the actual ΔX of the system compared to the maximal possible ΔX_{max}, gives information about the energy stored within the adsorbent.
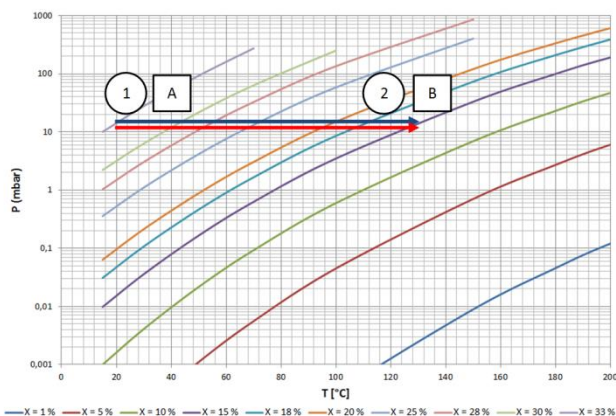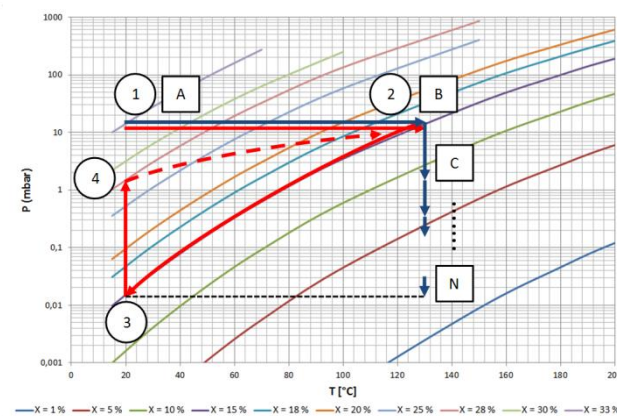
1) **Heating period during the day using pure adsorption.**

Main storage (blue line): Heating from A to B

Recharge unit (red line): Heating from 1 to 2
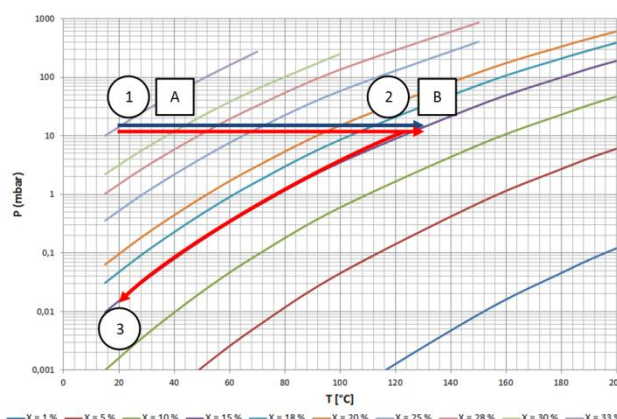
2) Isosteric cooling of the recharge unit during the night.

Main storage (blue line): Stays at point B

Recharge unit (red line): Isosteric cooling from 2 to 3
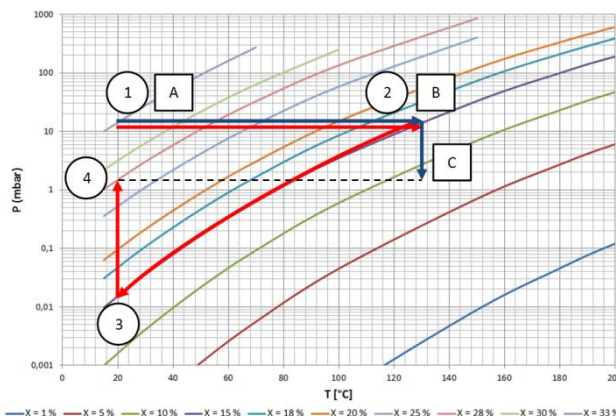
5) Connection of the two units with steam exchange

Main storage (blue line): Isothermal decrease in pressure and moisture content from B to C

Recharge unit (red line): Isothermal increase in pressure and moisture content from 3 to 4

4) Regeneration of the recharge unit.

Main storage (blue line): Stays at point C

Recharge unit (red line): Heating from 4 to 2

The cycle is then repeated until the main storage theoretically reaches point N, a significantly lower moisture content and therefore higher SOC than could be achieved with classic desorption alone (compare moisture content of B and N).

Figure 3-4: Schematic of the charge boost process with descriptions for each step in the order of **1):** Heating period during the day using pure adsorption. **2):** Isosteric cooling of the recharge unit during the night. **3):** Connection of the two units with steam exchange. **4):** Regeneration of the recharge unit.

This operating mode shows several advantages over pure desorption:

- The main storage unit can be charged further with charge boost than by normal desorption at the same temperatures. In return, this indicates that the lower temperatures are needed to reach a desired SOC. Combined with the fact that the solar-thermal collectors show better efficiency at low temperatures [31], this increases the efficiency of the whole process.

- As the SOC of the main storage unit can be higher than for pure desorption, less material is required. This reduces the cost and the space requirement of the system.

- The cycle efficiency[4] (for normal storages at one per year) increases, which reduces the specific cost of the system.

Based on the ideas of Mette [29] and Müller [30], experiments are conducted in this Master's Thesis to verify the theoretical predictions. Müller suggests the use of the charge boost technology to further charge a main storage unit which was already pre-charged during the summer period using pure adsorption.

Additionally, a new concept for the use of the charge boost technology during the winter months is developed by the author and then verified via further experiments. The expected advantages during winter are the colder temperatures outside which provide a lower temperature level for the heat sink and therefore could be profitably used for the charge boost technology. In order to perform these two experimental investigations, a testing plant built by Müller [30] at AEE Intec is used. It is adapted by the author to suit the needs for the test runs. In the following chapter, the status quo of the apparatus is described in detail.

---

[4] The cycle efficiency is defined as the ratio of the discharged thermal energy to the amount of energy input to the system [36]. $\eta_{cycle} = \dfrac{Q_{discharge}}{Q_{charge} + P_{aux,charge} + P_{aux,discharge}}$

4 Experimental setup for the proof of principle of the charge boost technology

4.1 Status quo of the testing plant

In this chapter, the testing plant as well as the measurement technology is described in detail (the plant was initially built by Müller [30] and later adapted by the author for the purposes of this thesis). Firstly, the hardware components and their respective connections are described. The whole plant is depicted in Figure 4-1.
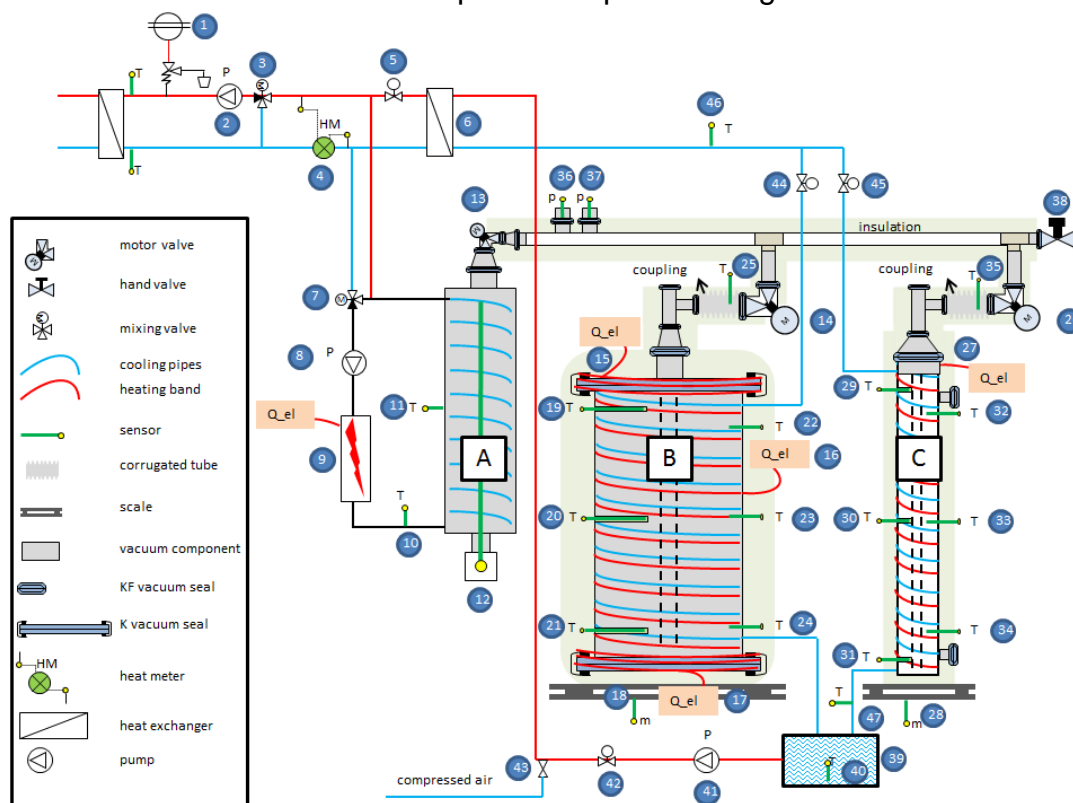

Figure 4-1: Schematic of testing plant at AEE Intec. **A)** Water storage/evaporator/condenser unit. **B)** main storage unit. **C)** recharge unit.

The three main parts of the plant are the water storage/evaporator/condenser unit[5] (A), the main storage unit (B) and the recharge unit (C). The solar collector is emulated in this experiment using electrical heating bands for the respective units. In order to provide a clear and structured description of the plant, it will be split into three segments for detailed explanation in the following chapters.

---

[5] This unit will be called condenser from here on.

4.1.1 Segment (A), primary cooling circuit and condenser

Primary cooling circuit

1. expansion tank
2. pump primary circuit
3. mixing valve primary circuit
4. heat meter
5. magnet valve
6. heat exchanger primary/secondary circuit
7. mixing valve condenser
8. pump condenser
9. heating rod
10. temperature sensor inlet condenser

Condenser

11. temperature sensor condenser
12. level indicator condenser
13. valve condenser
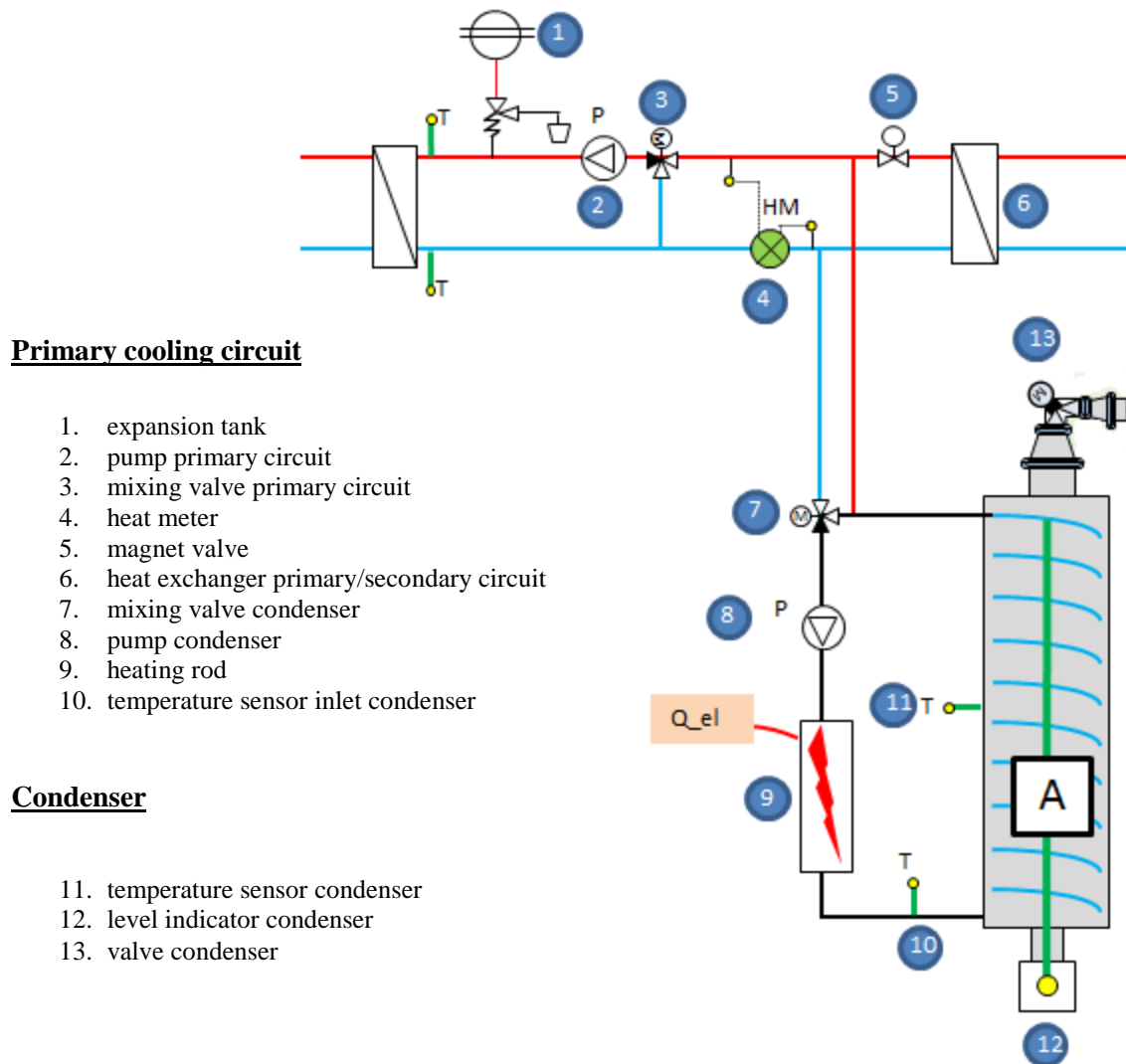
Figure 4-2: Schematic of segment (A), primary cooling circuit and condenser of the testing plant at AEE Intec.

The primary cooling circuit provides cold to the process and is connected to the compression refrigeration system of the laboratory at AEE Intec (heat exchanger on the left side of the system). The cooling circuit is operated with two pumps in total, one for the general system and one for the cycle around the condenser. The condenser cycle can be separated from the rest of the cooling circuit with the mixing valve condenser (7). This is necessary if the condenser is heated up with the heating rod (9) in order to avoid waste of energy by heating the complete cooling cycle electrically. The level indicator (12) is used in combination with a density correlation to determine the mass of water in the condenser unit. The condenser valve (13) connects the unit with the rest of the system.

4.1.2 Segment (B), main storage unit

Main storage unit

14. valve main storage unit
15. heating band storage top
16. heating band storage middle
17. heating band storage bottom
18. scale storage
19. temperature sensor inside storage top
20. temperature sensor inside storage middle
21. temperature sensor inside storage bottom
22. temperature sensor surface storage top
23. temperature sensor surface storage middle
24. temperature sensor surface storage bottom
25. temperature sensor storage coupling
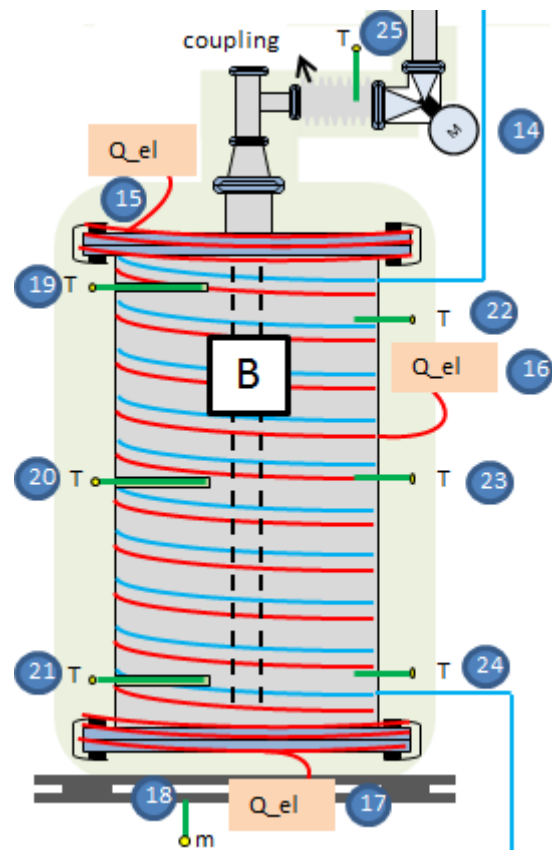
Figure 4-3: Schematic of segment (B), main storage unit.

The main storage unit is filled with zeolite 13XBF material as adsorbent. It is equipped with three separate electrical heating bands in order to provide an even temperature profile over the whole length of the vessel. Cooling is carried out with a combined air and water cooling in a copper pipe (air cooling above 100 °C and water cooling below 100 °C). The six temperature sensors measure the temperature profile inside the zeolite bed as well as the temperature profile on the surface of the unit. The storage scale monitors the mass of the storage unit. In combination with referenced masses of known humidity, the scale can also be used to determine the current moisture load of the zeolite. The main storage unit valve (14) connects the vessel with the rest of the system.

4.1.3 Segment (C), recharge unit and secondary cooling circuit
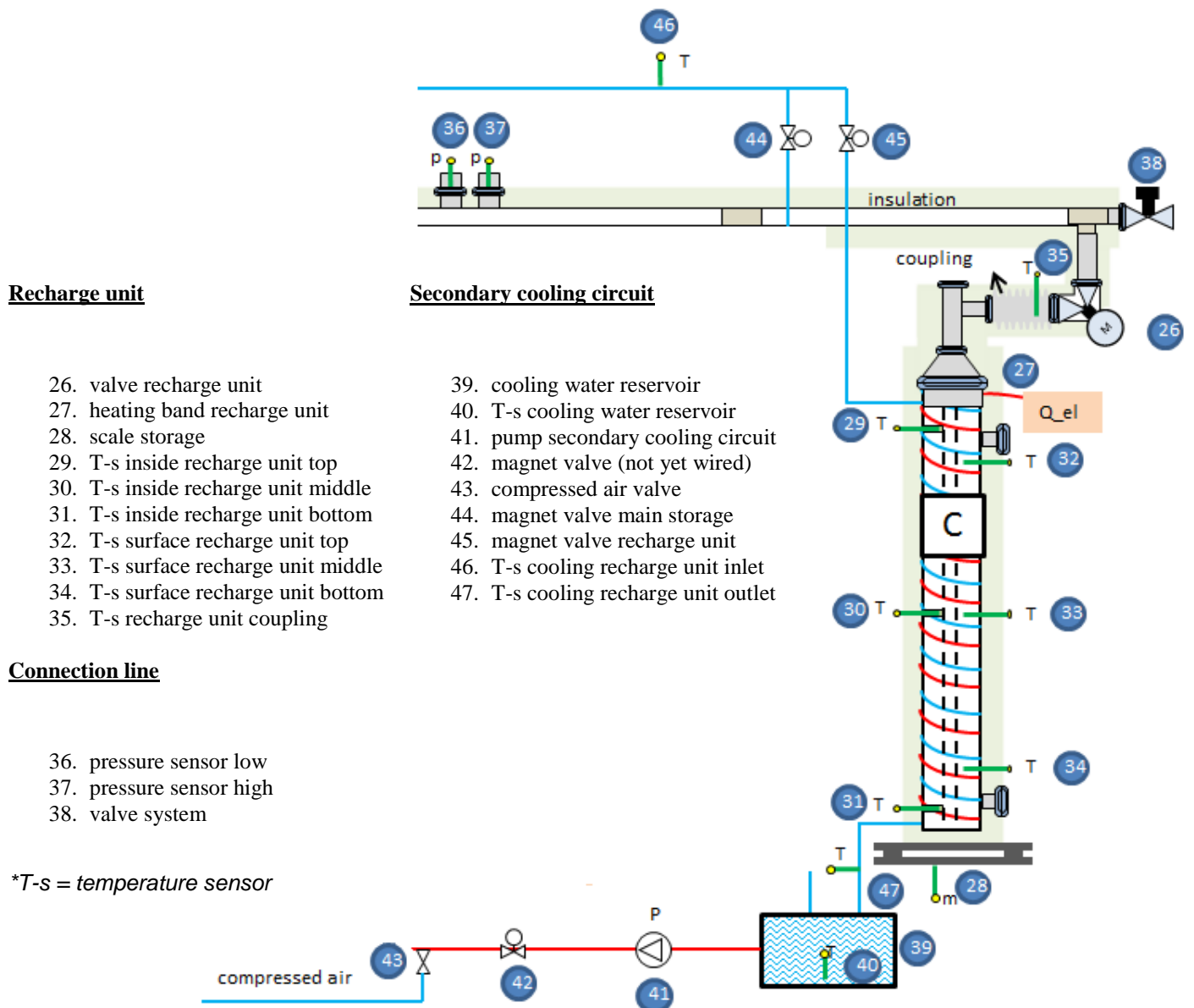
Figure 4-4: Schematic of segment (C), recharge unit and secondary cooling circuit.

Recharge unit

26. valve recharge unit
27. heating band recharge unit
28. scale storage
29. T-s inside recharge unit top
30. T-s inside recharge unit middle
31. T-s inside recharge unit bottom
32. T-s surface recharge unit top
33. T-s surface recharge unit middle
34. T-s surface recharge unit bottom
35. T-s recharge unit coupling

Secondary cooling circuit

39. cooling water reservoir
40. T-s cooling water reservoir
41. pump secondary cooling circuit
42. magnet valve (not yet wired)
43. compressed air valve
44. magnet valve main storage
45. magnet valve recharge unit
46. T-s cooling recharge unit inlet
47. T-s cooling recharge unit outlet

Connection line

36. pressure sensor low
37. pressure sensor high
38. valve system

T-s = temperature sensor

The recharge unit is filled with zeolite 13XBF as well. The solar radiation and the passive cooling at night are simulated with an electrical heating band and a copper cooling pipe (same principle as for the main storage unit). Although six temperature sensors are installed, only the middle and bottom ones are used during the experiments. This is due to the fact that the recharge unit heating band is too short and cannot be wrapped around the whole unit. Therefore the top end, where the least zeolite is stored, is left bare and the top temperature sensors are not taken into account in the process control system. The recharge unit valve (26) connects the vessel with the rest of the system.

In the connection line, two separate pressure sensors are installed. They have different measurement ranges (low = 0 – 100 mbar, high = 0 – 300 mbar). A logic query decides which pressure value is used in the process control system ($p < 10$ mbar = p_low; $p > 10$ mbar = p_high). In order to measure the pressure in the respective vessels, they have to be connected with the connection line while all other units are closed off. The system valve (38) is the connection to the ambient atmosphere and should be closed permanently after evacuating.

As mentioned in the description of the main storage unit, the cooling system is a combined air and water cooling system. This is necessary because water would evaporate in the cooling pipes at temperatures above 100 °C, whereas a pure air cooling system would not be able to provide the required cooling power for the process. During air cooling, the compressed air valve (43) is opened. Pressured air provided by the laboratory compressor flows through the cooling tubes and leaves them through the cooling water reservoir (39) to the ambient. For water cooling, the compressed air valve is closed and the secondary cooling circuit pump (41) starts to distribute the cooling water within the system. The cooling water is cooled in the primary/secondary heat exchanger (6, see segment A). The magnet valves (44) and (45) are used to define which vessel is being cooled. Since only magnet valves and no mixing valves are used, it is impossible to determine the ratio of the two mass flows of the main storage and the recharge unit if both valves are opened simultaneously. Therefore, it is only possible to cool the two units consecutively. In Figure 4-5, a photograph of the whole plant is depicted.
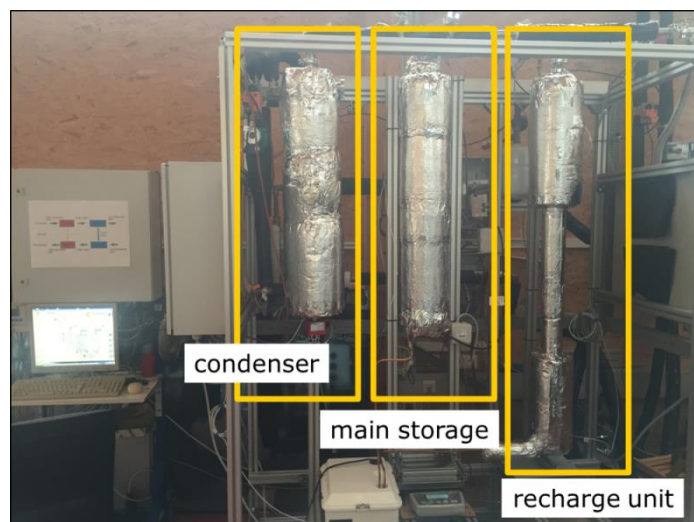
Figure 4-5: Picture of the testing plant at AEE Intec with condenser (left),
main storage (middle) and recharge unit (right).

5 Proof of principle of the charge boost technology via experiments

5.1 Experimental procedure

The goal of the first run of experiments in the laboratory is to verify the feasibility of the charge boost technology as suggested by Mette [29] and Müller [30] (see chapter 3.2). In order to do this, the existing testing plant at AEE Intec is used to determine whether the charge boost process can increase the SOC of an already charged CSESS. To be able to compare the experiments with each other, fixed high and low temperature levels have to be chosen for the system. Additionally, it was suggested to test the method with two different high temperature levels for the main storage unit and the recharge unit. This setup is expected to have the following advantages in real life applications:

- Sensible heat loss would be reduced as the hotter recharge unit has less mass than the cooler main storage.

- If only a moderate collector area is available, the big heat capacity of the main storage only allows for comparably low temperatures. As the recharge unit has smaller mass and consecutively a smaller heat capacity, it can be heated to higher temperatures, which in return makes the recharge technology attractive to use.

The chosen temperature levels for the experiments are shown in Table 5-1.

Table 5-1: Temperature levels for the first run of experiments for the proof of principle of the charge boost technology.

Temperature level	T [°C]	Temperature level	T [°C]
Desorption recharge unit	140	Charge boost recharge unit	140
Desorption main storage	60	Charge boost main storage	60
Regeneration recharge unit	16	Condenser	16

Since the recharge procedure not only involves a lot of accurate switches in the process control system but also requires a significant amount of time, an automatic process control program is established. It consists of eight different operating modes which are connected to each other via break criterions. The general experimental procedure as well as the break criterions and the respective operating modes are defined in the following. The flow sheet of the experimental process is depicted in Figure 5-1.
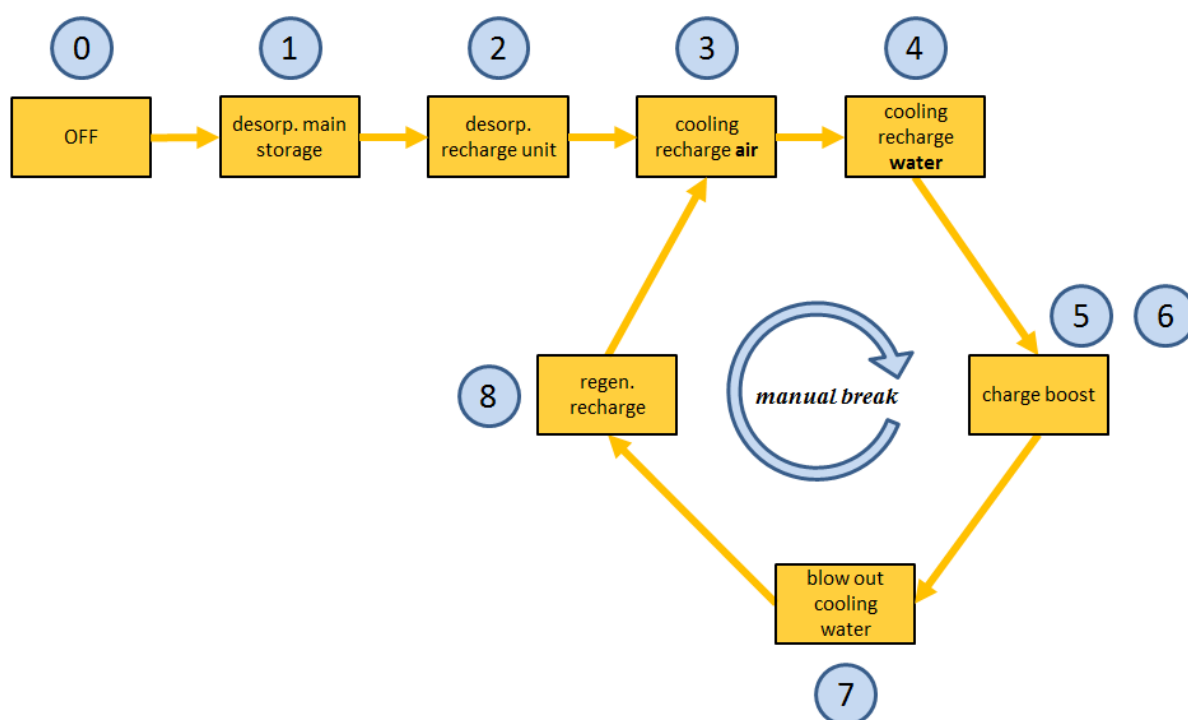
Figure 5-1: Schematic for the automatic process control program. **0)** Off. **1)** Desorption of the main storage. **2)** Desorption of the recharge unit. **3)** Cooling of the recharge unit with air. **4)** Cooling of the recharge unit with water. **5,6)** Charge boost. **7)** Blow out of the cooling water from the recharge unit cooling system. **8)** Regeneration of the recharge unit.

This process represents the recharge cycle at the end of summer. Main storage and recharge unit are heated and charged simultaneously with solar radiation (1) and (2). The maximum energy density that can be reached is defined by the peak solar temperature in summer as well as the lowest possible pressure in the condenser unit (see chapter 3.1). As soon as the main storage unit cannot be dried any further with mere (simulated) solar radiation, the recharge cycle starts. The dried recharge unit undergoes an isosteric cooling process during which temperature and pressure decrease while the moisture content in the zeolite stays constant (3) and (4).

During the recharge process (5) and (6), the cooled recharge unit is connected with the main storage unit. Steam is conducted from the high pressure main storage unit to the low pressure recharge unit until equilibrium is reached. After separating the two vessels, the recharge unit is regenerated with (simulated) solar radiation (8) and the cycle from (3) to (8) starts again. This loop is executed until a manual break command terminates the whole experimental procedure.

Since the different operating modes of the system are now described, the respective breaking criteria will be stated in the following paragraph.
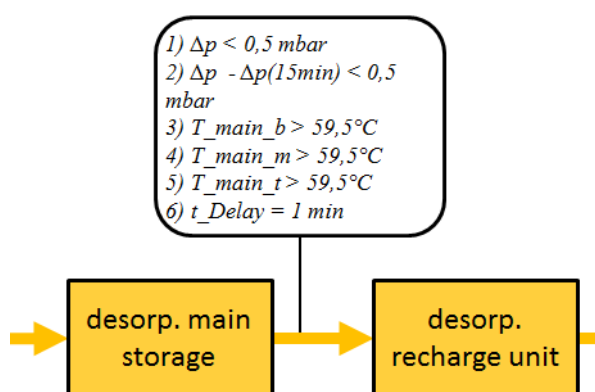
Figure 5-2: Breaking criteria between mode (1) and (2) listed and numbered in the white label.

Figure 5-2 depicts the break criteria between mode (1) and (2). The first two criteria are in regard of the pressure and ensure that the desorption process is finished. Breaking criterion C1[6] demands a pressure gradient below a certain threshold between main storage and condenser, whereas C2 checks whether the process reached a stable equilibrium by comparing the Δp of the last 15 minutes. The following criteria C3, C4 and C5 demand an equal temperature profile in the main storage unit, with the indices b_bottom, m_middle and t_top of the vessel. The last criterion C6 is a simple time delay that forces the program to wait at least one minute after all conditions are met before it switches to the next operating mode. This guarantees that the equilibrium is stable and not only present for one second.

---

[6] From here on the respective breaking criteria will be labelled as C1 for the first one, C2 for the second one and so on.
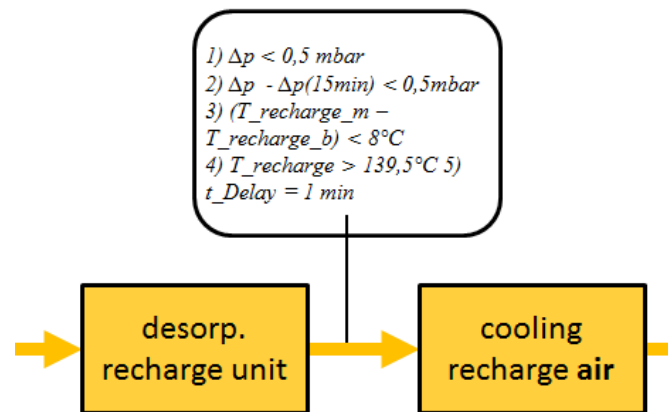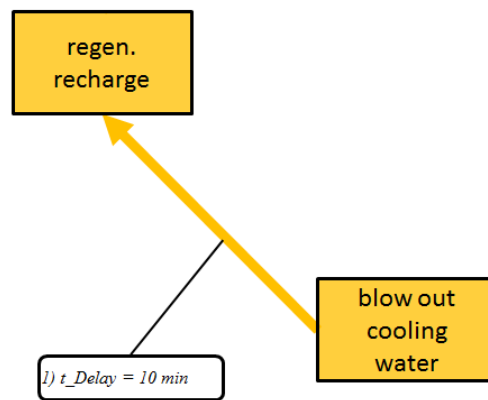
Figure 5-3: Breaking criteria between mode (2) and (3) listed and numbered in the white label.

The break criteria between mode (2) and (3) are very similar to those mentioned beforehand. The main difference lies in the temperature criteria C3 and C4. C3 asks for an average temperature of the recharge unit to be above a certain threshold whereas C4 ensures an even temperature profile by comparing the hottest part of the vessel (m_middle) with the coldest one (b_bottom) and demanding a maximum ΔT of <8 °C.
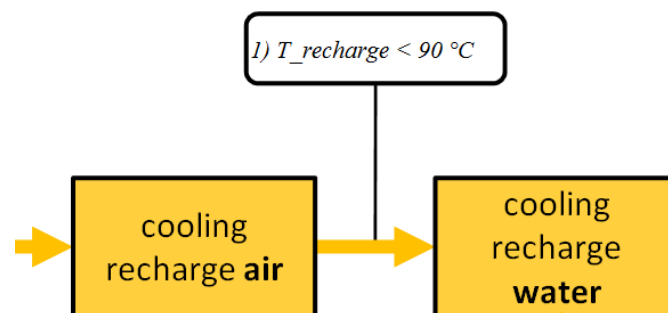
Figure 5-4: Breaking criterion between mode (3) and (4) listed and numbered in the white label.

The break criterion between the two cooling modes (3) and (4) demands an average recharge unit temperature below 90 °C in order to guarantee that the cooling water in step (4) will not evaporate inside the copper tubes.
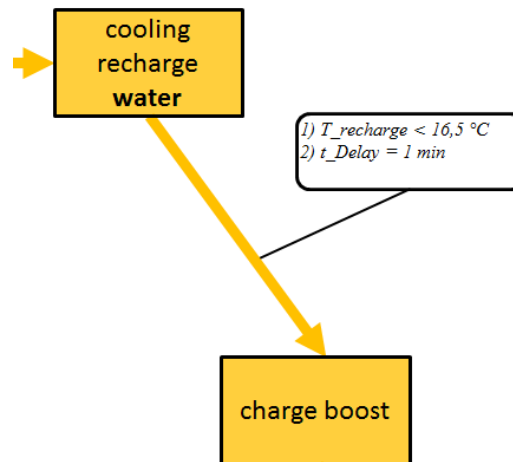
Figure 5-5: Breaking criteria between mode (4) and
(5,6) listed and numbered in the white label.

C1 triggers when the average temperature of the recharge unit drops below 16,5 °C
and thereby ensures a sufficient cooling of the vessel. C2 represents the usual time
delay condition.
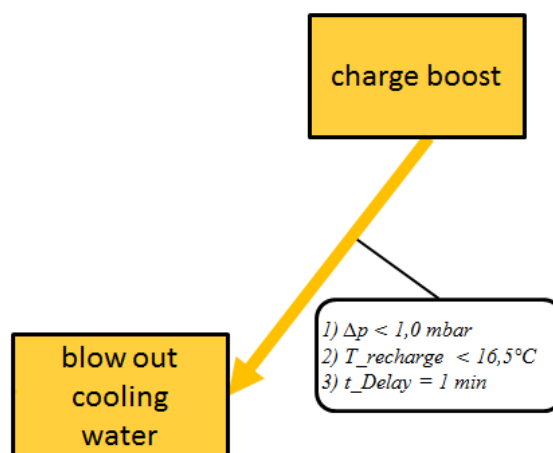
Figure 5-6: Breaking criteria between mode (5,6) and (7) listed
and numbered in the white label.

C1 requires a Δp below 1 mbar between the main storage unit and the recharge unit.
The second criterion C2 is necessary to ensure that the adsorbing recharge unit does
not heat up to a temperature above 16,5 °C, but rather has a temperature below the
threshold at the end of the process. C3 again represents the time delay.

Figure 5-7: Breaking criterion between mode (7) and
(8) listed and numbered in the white label.

The time delay criterion between operating modes (7) and (8) is longer than the ones used beforehand. This is due to the fact that the residual amount of water in the cooling tubes after the blow out cannot be measured. Therefore, a time delay of 10 minutes is installed to ensure that the tubes are free of water. The duration of the interval was chosen based on empirical observations (see chapter 5.2).
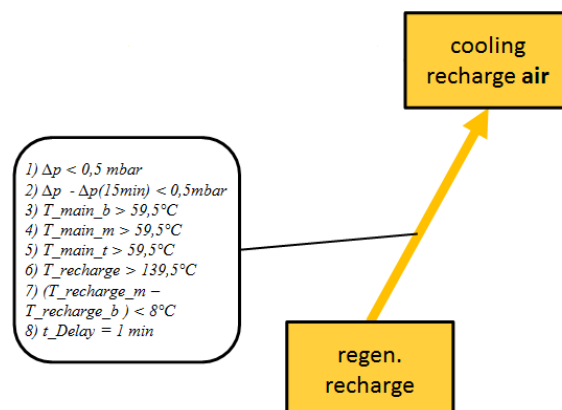
Figure 5-8: Breaking criteria between mode (8) and
(3) listed and numbered in the white label.

Between the last step of the recharge loop and the start of the next iteration, the system checks several parameters in order to provide stable starting conditions for each cycle. C1 and C2 are already known and guarantee that the regenerating recharge unit and the condenser are in stable equilibrium. The criteria C3, C4 and C5 check whether the temperature in the desorbed main storage unit is within the desired range. Criteria C6 and C7 fulfil the same purpose concerning the recharge unit. C8 is the known time delay criterion.

As well as the 8 defined operating modes, also an automatic pressure measurement is installed. As only one point of the plant (the steam canal) is equipped with pressure sensors, the respective vessels need to be connected to the canal in order to measure their pressure. This however influences the operating parameters as the steam canal does not have the same pressure or temperature as the vessels. Therefore, the pressure measurement is not carried out every 10 minutes for each of the three vessels, but rather only for the vessels in use during the current operating mode. For example, during the desorbing of the main storage unit with the condenser (1), the pressure in the recharge unit is not measured as it is not used in the process. By implementing this refined measurement technique, the influence of the pressure measurement on the process could be reduced significantly.

5.2 Preparations for the experiment

Before the experiments can be started, the plant needs to be checked for several parameters and has to be adjusted accordingly.

5.2.1 Mass-volume correlation in the evaporator/condenser unit

The mass measurement of the condenser is carried out with a level indicator and is based on a mathematical correlation between volume and mass, using the temperature dependent density of distilled water. Müller already established such a function in his Master's thesis [30]. The condenser was tested nevertheless in order to ensure the function was viable to use in the experiments. This was done by filling the condenser unit with known mass units of distilled water and noting the measured levels within the device. The fit used by Müller was verified. The function used during the experiments equals:

$$V_{condenser}[ml] = 1{,}6194 * R[\Omega] + 1281{,}8 \qquad (5.1)$$

5.2.2 Evacuating of the plant and determination of the leakage rate

As the experiments take place at vacuum conditions, the whole device needs to be evacuated beforehand. Since the experiments will run for a longer period of time, the leakage rate of the plant has to be below a certain threshold. This leakage rate is stated in $\frac{mbar*l}{s}$ and calculated with the following formula:

$$L_R = \frac{\Delta p * V_{plant}}{time}$$

(5.2)

The threshold for testing plants at AEE Intec is $L_R < 10^{-5}$, which was reached during the vacuum test.

5.2.3 Removing inert gases from the system

As all three vessels as well as the steam canal had to be opened during the adapting process of the testing plant, air came in contact with the zeolite inside the units. Not only can steam be adsorbed on the zeolite but inert gases from the ambient air as well. They usually have a lower affinity for the adsorbent which means that they become gaseous again when they are replaced by steam on the solid surface. Since they cannot be removed from the system by condensation, like steam, the inert gases increase the pressure within the experimental setup during the process. This change in pressure needs to be prevented as it would lead to varying operating conditions for the whole experiment. Therefore, the inert gases which are adsorbed on the zeolite need to be removed beforehand. This is achieved by heating up the two adsorbent containing units, the main storage and the recharge unit, to a comparably high temperature (140 °C). After this process, the removed inert gases can be withdrawn with the vacuum pump[7]. In order to determine whether all inert gases are removed, the pressure in the steam canal can be compared to the water vapour pressure corresponding to the temperature in the condenser unit (with open condenser). If these two values match, no inert gases should be present within the apparatus.

---

[7] The inert gases should be moved to the condenser before they are extracted. The main storage and the recharge unit should be closed during this process. This is due to the fact that opening the two units directly to the vacuum pump would cause additional water to desorb from the material. This steam would damage the vacuum pump severely.

5.2.4 Testing of the cooling system

The newly installed combined air and water cooling system needed to be tested as well. Firstly, the amount of time needed to blow out the residual water from the water cooling was determined. This was done by measuring the mass of the respective unit without water, and subsequently with cooling water. The pressured air was activated, so that the unit eventually showed the same mass as the initial measurement, which means that all residual water has been removed. During the measurements a problem with the experimental setup was discovered. As long as the pressured air was active, the mass of the unit was slightly lower than without pressured air flow. A possible reason for this phenomenon could be the blowback of the pressured air hitting the water in the storage tank. The experimental results showed that, for a time interval of 3 minutes, the original mass was almost reached. In order to guarantee the removal of all water for every time this arguably volatile process is conducted, a time interval of 10 minutes was chosen.

5.2.5 Pre-conditioning of the plant

Every single experiment should start from the same conditions to provide a reliable basis for comparison. Therefore, the moisture load of the adsorbent is measured via Δm values. This means that the initial condition of the zeolite adsorbent has to be known as well in order to be able to correctly compute the moisture loads.
For this reason, a pre-conditioning of the whole experimental plant is necessary to ensure that every process starts with the same- and known starting conditions. The chosen method for this series of experiments was to wet the main storage unit and the recharge unit completely. This represents the condition at the end of the winter when the total adsorbing potential has been exhausted.

To achieve this state, the connection valves of the condenser, main storage unit and recharge unit are opened simultaneously. In the next step the condenser is heated up until it almost reaches the temperature of the zeolite filled units. Its temperature should never exceed the one of the two other vessels as the condenser needs to be the coldest component of the system in order to prevent unwanted condensation. This state is held until the temperature and mass of the main storage unit and the recharge unit do not vary anymore. This means that they adsorbed the maximum

amount of water vapour from the condenser and have reached their adsorption capacity, hence being absolutely wet. The process can be sped up significantly by cooling the two adsorbing units, as the adsorption energy causes an increase in vessel temperature, which slows down the adsorption process.

During the first run of this procedure, it became apparent that the time scale was significantly longer than anticipated. Pre-conditioning for 24 hours was not enough to reach equilibrium. Therefore, the pre-conditioning was done during the work day, the duration ranging from 7 to 5 hours. After that, the respective experiment was started.

Other measures and simplifications have been used to compensate for the missing pre-conditioning. The moisture load of the material can not only be determined by Δm values and a known reference masses, but also by measuring the pressure and temperature in the vessels as they are connected by the theorems of adsorption. However, this leads to the loss of a possible cross reference check.

5.3 Experimental results

In total, ten experiments were conducted during the first testing period of this Master's thesis. Especially in the earlier experiments, unexpected errors occurred, which rendered the results scientifically useless (marked with an * in Table 5-2), whilst at least providing useful information about the behaviour of the plant. Therefore, a complete list with all ten experiments as well as special remarks is shown in Table 5-2.

Table 5-2: List of all ten experiments performed for the proof of principle for the charge boost technology with additional remarks regarding the experimental results.

No.	Remarks
1	Problems with the main storage temperature (*)
2	Problems with the automatic control system (*)
3	Problems with the automatic control system (*)
4	First successful run, pressure fluctuations (*)
5	Pressure fluctuations, fluctuations of the main storage mass, mass of the recharge unit decreases (*)
6	No pressure fluctuations but increasing pressure with every charge boost step, mass of the recharge unit decreases (*)
7	Pressure increases with every charge boost step, mass of the main storage decreases, mass of the recharge unit fluctuates
8	Pressure increases with first recharge steps but then decreases to desired level, masses of main storage and recharge unit decreases, mass of the condenser increases
9	Constant pressure levels during all charge boost steps, mass of the main storage decreases/fluctuates, mass of the recharge unit is constant
10	Pressure increase during the charge boost steps, mass of the recharge unit decreases, mass of the main storage unit increases

As only experiments 7 to 10 yielded scientifically viable results, only these 4 test runs shall be discussed in detail, regarding the behaviour of pressure, temperature and mass/moisture content.

5.3.1 Experiment 7

The pressure levels for all three vessels in experiment 7 are depicted in Figure 5-9.
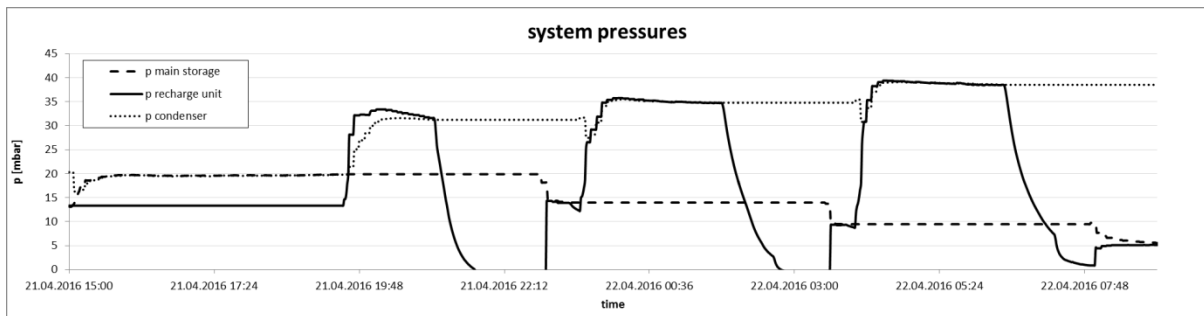
Figure 5-9: Pressure levels over the course of experiment 7 for all three vessels.

The pressure of the main storage unit shows the desired course, starting at 20 mbar and decreasing with every charge boost step. However, the pressure of the recharge unit as well as the condenser unit increases over the course of the experiment. This disagrees with the theoretical expectations. An analysis of possible causes is carried out in chapter 5.4.1. It can be stated that the increasing pressure in the recharge and condenser unit reduce the effectiveness of the whole process.

The temperature levels of the main storage unit and recharge unit are depicted in Figure 5-10.
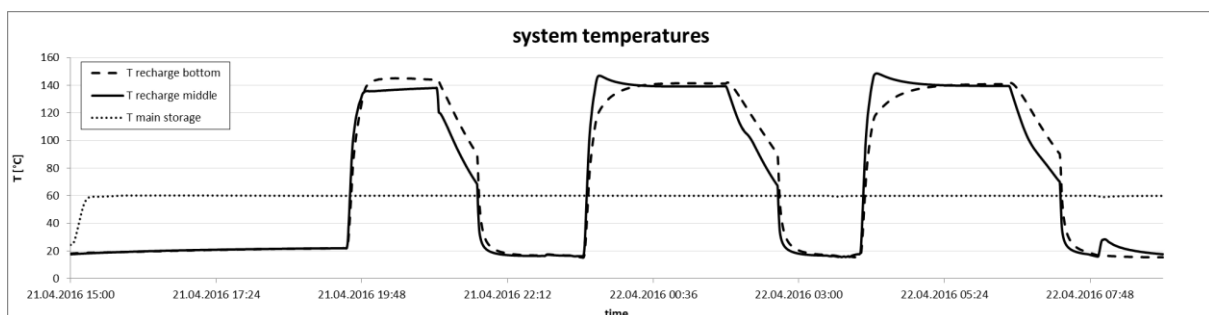
Figure 5-10: Temperature levels over the course of experiment 7 for main storage unit and recharge unit.

The temperature sensor at the top of the recharge unit is excluded again for the same reason as before. The temperature of the main storage is only plotted for the middle temperature sensor. This is justified as the main storage temperature is stable in all conducted experiments except for experiment 1. The temperature of the condenser is not plotted as this value is stable throughout all experiments as well. The temperature courses for experiment 7 are following the theoretical predictions.

The masses of the main storage and the recharge unit are depicted in Figure 5-11 with two differently scaled axes.
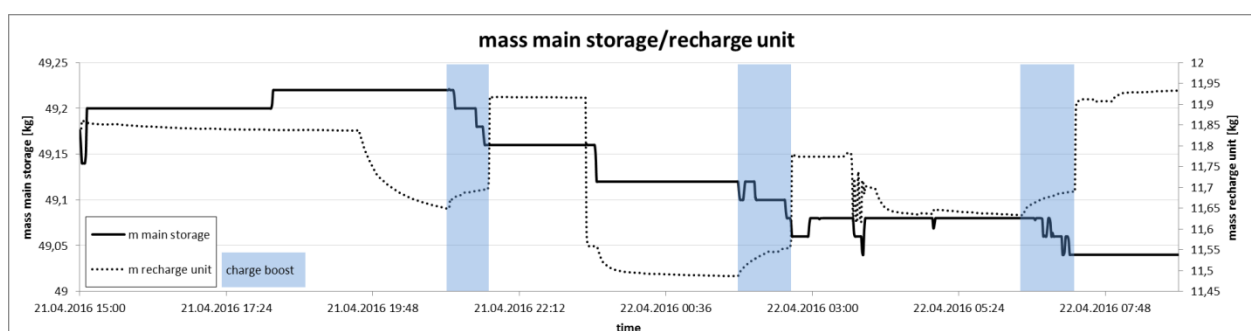
Figure 5-11: Masses of the main storage unit and the recharge unit over the course of experiment 7 with two differently scaled axes (mass main storage left axis, mass recharge unit right axis). Regions of charge boost are marked with blue squares.

The mass of the main storage unit is decreasing over time which is corresponding to the theoretical predictions. However, the fluctuations which occur aside from the charge boost steps cannot be justified (charge boost regions are marked with blue squares in Figure 5-11. The mass of the recharge unit also shows the predicted behaviour, with the middle peak being too low in comparison to the other two peaks as all peaks should have approximately the same height. This may be due to the fact that the first desorbing process of the recharge unit is not carried out to its full potential. As it will be discussed in detail in chapter 5.4.1, problems occurred regarding the pressure in the system. This caused a pressure equilibrium which was at a higher level than the saturation vapour pressure at the given system temperature, resulting in a reduction of the adsorption potential.

The gain in SOC for every charge boost cycle is calculated from the initial condition of the main storage and the Δm of each charge boost step. The initial condition is not determined by a reference mass as mentioned in chapter 5.2.5, but rather with the temperature and pressure of the main storage unit along with the formula of Dubinin Astakhov [22] (see chapter 2.4.2).

$$X = X_{max} * exp\left[\left(-\frac{RT}{EM} * ln\left(\frac{p_S}{p}\right)\right)^n\right]$$

(2.11)

This formula is also used to determine the SOC after each charge boost step in order to provide a cross reference for the obtained values from the mass measurements. The results are shown in Table 5-3 (the status always refers to the condition after the respective cycle is finished).

Table 5-3: List of values for moisture load X and SOC for the initial condition and each charge boost cycle. The index _calculated refers to the value obtained from purely theoretical calculations while the index _measured marks values which have been calculated using experimental data.

Status	X_calculated	X_measured	SOC_calculated	SOC_measured
Start	27,83	27,83	0,15	0,1544
Cycle 1	26,77	27,82	0,19	0,1546
Cycle 2	25,52	27,81	0,22	0,1547
Cycle 3	23,77	27,81	0,28	0,1548

It is apparent that the calculated values greatly differ from the measured ones. There are three general possibilities which could explain this behaviour: The pressure used for the calculation is not measured correctly; the mass used for the Δm determination is not measured correctly or both measurements are faulty. To evaluate which data is correct, three different methods are compared in Table 5-4; the Δm method, the calculation based on pressure and temperature of the vessels and a completely theoretical calculation, which only uses the starting values of the experiment and generates the rest of the data via the Dubinin-Astakhov equation (see equ. 2.11) [22].

Table 5-4: Comparison of three different approaches to compute the change in moisture content ΔX in %. The **Δm method** uses the experimental values for the change of mass and the Dubinin-Astakhov equation to calculate ΔX. The **T,p method** uses the experimental values for temperature and pressure along with the Dubinin-Astakhov equation to calculate ΔX. The **theor. calc.** only uses the initial condition and then proceeds to calculate all other values purely on a theoretical basis using the Dubinin-Astakhov equation as well.

Vessel/Cycle	ΔX *Δm method* [%]	ΔX *T,p method* [%]	ΔX *theor. calc.* [%]
Main storage/1	0	1,08	1,18
Main storage/2	0,0076	1,27	1,13
Main storage/3	0,0015	1,75	1,09
Recharge unit/1	0,0780	12,19	12,18
Recharge unit/2	12,3090	11,71	11,77
Recharge unit/3	2,000	10,46	11,14

The values show that the method using the T,p measurement fits the theoretical predictions much better than the Δm values. The exception is the value for the last charge boost step. In this case, the purely theoretical calculations predict a lower ΔX than the value obtained via the T,p measurements. However, this can be justified by noting that the experiment was stopped before the last recharge cycle could finish completely, resulting in a greater ΔX (no pressure equilibrium in the steam canal).

The Δm values on the other hand show results that do not compare to any of the other two methods and have no reasonable structure. This leads to the assumption that this measurement is not suited to evaluate the processes of the plant. In order to further investigate this assumption, the amount of moved water is calculated. Due to mass conservation, the mass of water leaving the main storage must be equal to the mass of water entering the recharge unit. Again, the values for the mass of water are determined by all three methods.

For the Δm method, no additional calculations have to be made. The other two approaches calculate the mass of water based on the change in moisture content along with the mass of zeolite in the respective units, see formula 5.3:

$$\Delta m_{water} = m_{zeolite} * (X_{start} - X_{end})$$
(5.3)

The results are shown in Table 5-5.

Table 5-5: Comparison of three different approaches to compute the change in mass Δm in g. The **Δm method** uses the experimental values for the change of mass and the Dubinin-Astakhov equation to calculate ΔX. The **T,p method** uses the experimental values for temperature and pressure along with the Dubinin-Astakhov equation to calculate ΔX. The **theor. calc.** only uses the initial condition and then proceeds to calculate all other values purely on a theoretical basis using the Dubinin-Astakhov equation as well.

Vessel	Δm *Δm method* [g]	Δm *T,p method* [g]	Δm *theor. calc.* [g]
Main storage/1	0	141	156
Main storage/2	100	166	149
Main storage/3	20	229	142
Recharge unit/1	1	155	155
Recharge unit/2	156	149	150
Recharge unit/3	25,5	133	142

Again, the T,p method and the theoretical calculations show similar results, with the third cycle being the exception because it was stopped before it could reach equilibrium. The values determined by the Δm method show different behaviour. The two calculating methods are in adequate agreement with mass conservation, as the values for the different cycles of both vessels are almost the same. However, this is also true for the Δm method to some extent. Nevertheless, from this point on the T,p method will be used for the assessment of the experimental results as it appears to be more consistent.

5.3.2 Experiment 8

Experiment 8 was a long term experiment and lasted four days instead of the one day period of setup 7. The pressure levels for all three vessels are depicted in Figure 5-12.
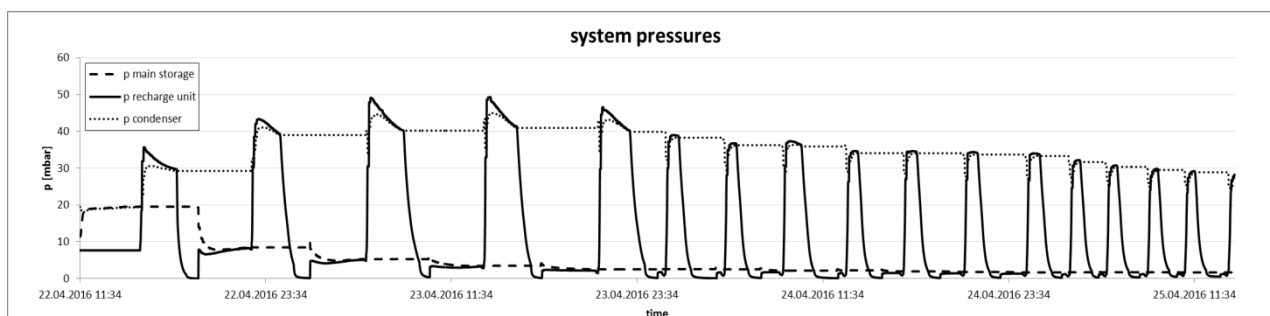
Figure 5-12: Pressure levels over the course of experiment 8 for all three vessels.

As observed in experiment 7, the pressure in the system increases with every recharge cycle. However, after the fourth cycle is completed, the pressure starts to decrease again unexpectedly. Possible reasons for this behaviour will be discussed in chapter 5.4.1. Furthermore, the width of the peaks, representing the periods of heating in the recharge unit, becomes smaller, which was not anticipated either. A possible reason for this behaviour may be the consecutive drop in pressure of the main unit. A lower pressure gradient means less moved water, hence the amount of adsorbed water in the recharge unit decreases as well. This leads to a lower energy requirement during the heating period, which causes the peaks to loose width. This assumption can be backed up by a calculation using the formula of Dubinin-Astakhov [22]. The amount of ΔX decreases with each charge boost step as expected. The respective results of the calculations are provided along with an accompanying graph in Figure 5-13.

Cycle index	ΔX [%]	Cycle index	ΔX [%]
1	1,18	5	0,97
2	1,13	6	0,9
3	1,09	7	0,84
4	1,03	8	0,78
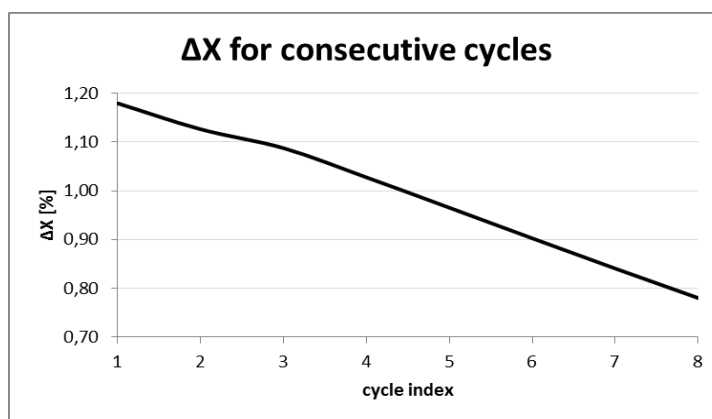
Figure 5-13: Calculation of ΔX using the Dubinin-Astakhov equation. Exact values in table **(left)** alongside a plot of the data points **(right)**.

The temperature levels of the main storage unit and recharge unit are depicted in Figure 5-14.
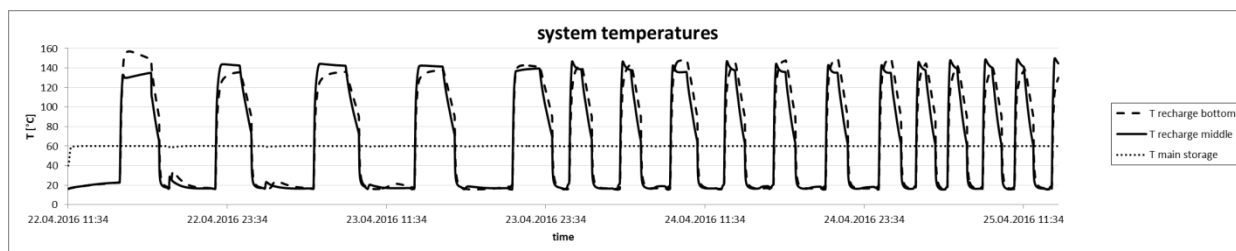
Figure 5-14: Temperature levels over the course of experiment 8 for main storage unit and recharge unit.

The temperature courses for experiment 8 fulfil the theoretical predictions. The decreasing height of the smaller peaks in-between the big ones show that the charge boost efficiency is reduced with every consecutive cycle, as stated before.

The masses of the main storage and the recharge unit are depicted in Figure 5-15 with two different axes.
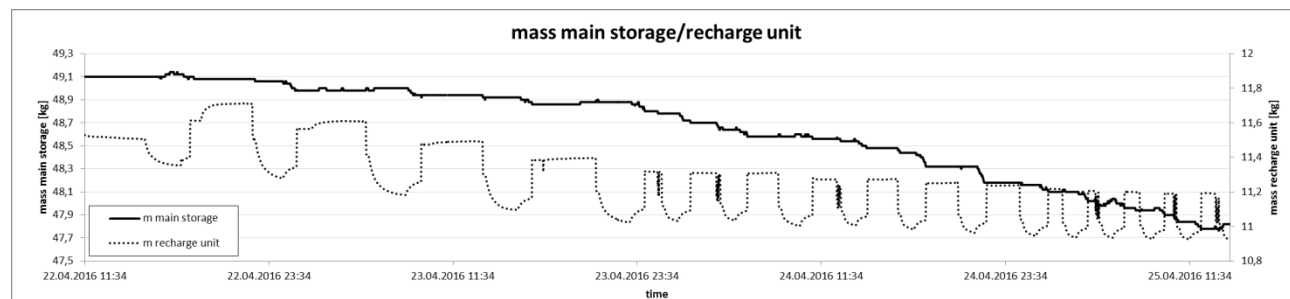
Figure 5-15: Masses of the main storage unit and the recharge unit over the course of experiment 8 with two differently scaled axes (mass main storage left axis, mass recharge unit right axis).

The mass of the main storage unit is decreasing over time which is corresponding to the theoretical predictions. Under close inspection it is apparent that the mass decrease occurs in steps during the charge boost process. The mass of the recharge unit however should be constant for each cycle which is not true for this experiment. A possible reason for this will be discussed in chapter 5.4.2.

As discussed in the chapter concerning experiment 7, the moisture content in the main storage will be determined via the T,p-method over the course of the process. The results will be compared again to the theoretically calculated values, this time graphically in Figure 5-16.
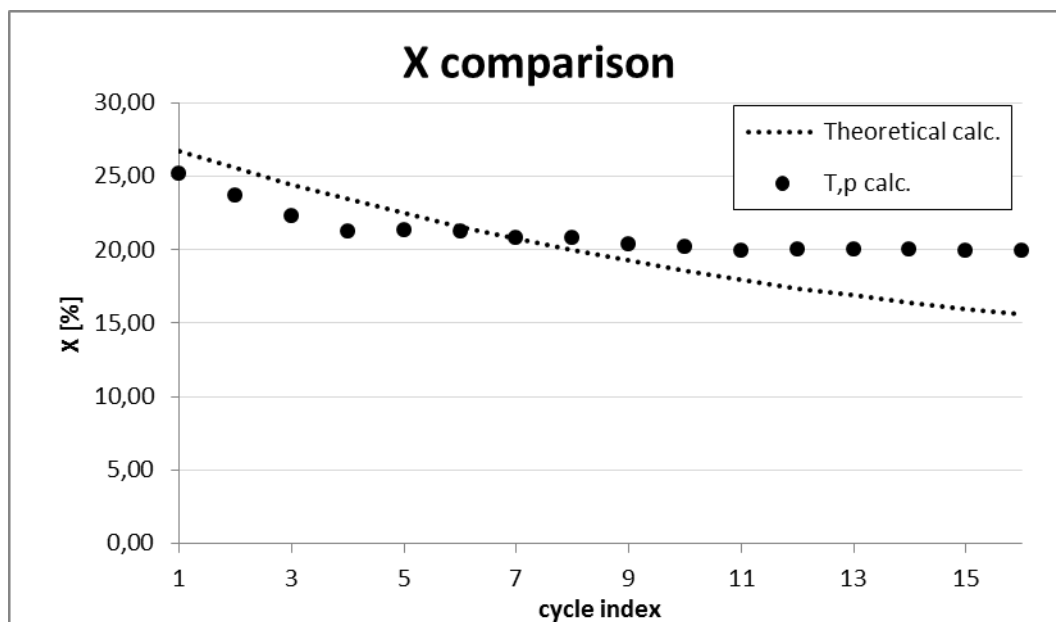
Figure 5-16: Comparison of the calculated X values using a purely theoretical calculation (dotted line) and the experimental data for temperature and pressure (black dots).

Figure 5-16 shows that the measured values of the T,p method fit the purely theoretical results, with the threshold being at a higher level than expected. This higher final value of moisture content may have been caused by the presence of inert gases within the system (detailed discussion in chapter 5.4.1).

5.3.3 Experiment 9

The pressure levels for all three vessels are depicted in Figure 5-17.
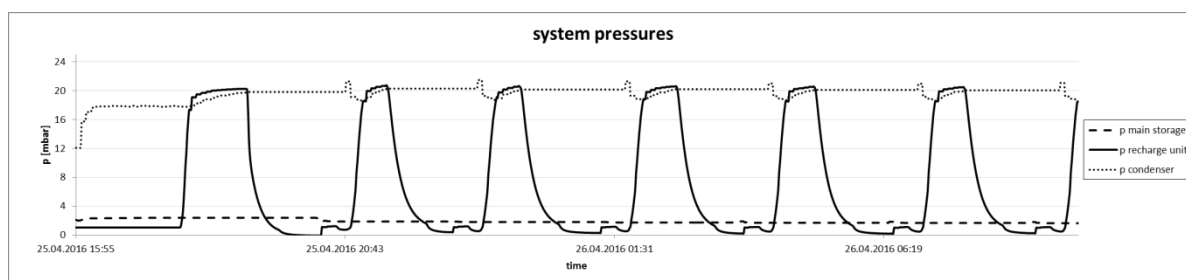
Figure 5-17: Pressure levels over the course of experiment 9 for all three vessels.

Experiment 9 shows the ideal pressure profile. It matches the theoretical predictions, the maximum pressure is about 20 mbar, which corresponds to the saturation vapour pressure at the given condenser temperature. Furthermore, the main storage unit loses pressure during each charge boost step. Although no setup changes were carried out in-between experiment 8 and 9, no increase in pressure occurred. Possible reasons for this will be discussed in chapter 5.4.1. It has to be pointed out though, that the main storage unit has a starting pressure that is below the anticipated 20 mbar. The reason for it being so low will be discussed in the temperature section of this chapter.

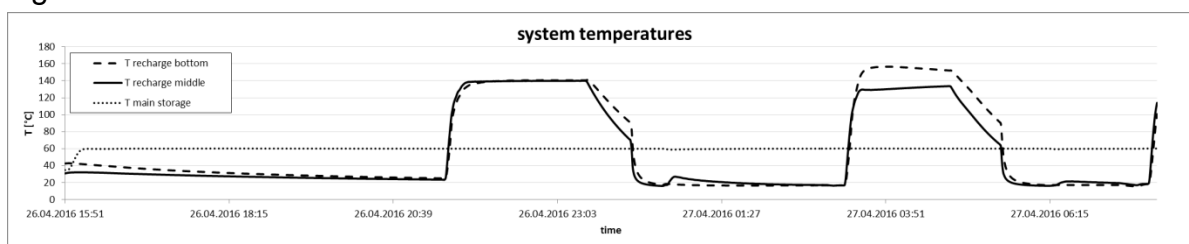The temperature levels of the main storage unit and recharge unit are depicted in Figure 5-18.
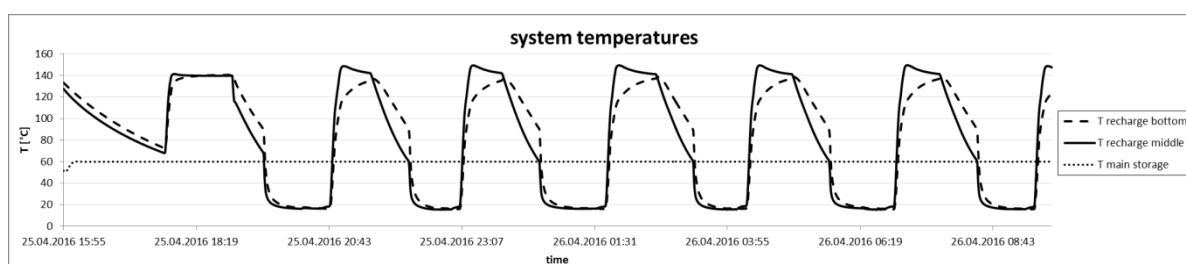
Figure 5-18: Temperature levels over the course of experiment 9 for main storage unit and recharge unit.

The temperature profile looks optimal at a first glance. However, two significant characteristics have to be pointed out. Firstly, the starting temperature of the recharge unit in the experiment is too high as it should be at around 20 °C which equals the average temperature in the laboratory. This is most likely the result of a pre-conditioning step that was not carried out correctly. Secondly, no significant increase in temperature can be observed during the charge boost step (no small peaks in-

between the large ones). This could mean that no water was moved and hence no adsorption energy was released in the recharge unit. This assumption will be tested via the investigation of the respective ΔX values.

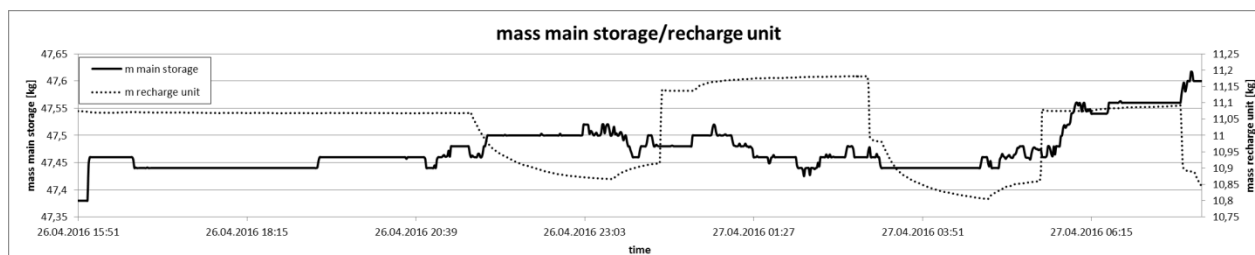The masses of the main storage and the recharge unit are depicted in Figure 5-19 with two different axes.
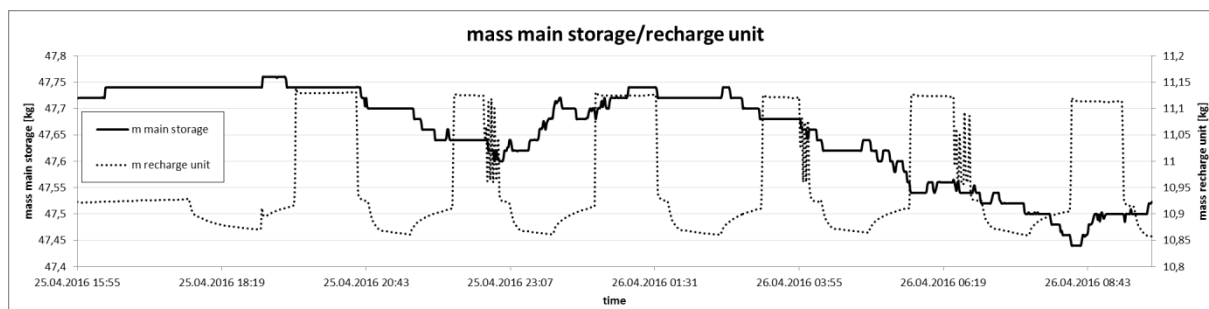
Figure 5-19: Masses of the main storage unit and the recharge unit over the course of experiment 9 with two differently scaled axes (mass main storage left axis, mass recharge unit right axis).

The mass of the main storage unit shows fluctuating behaviour. Although it decreases over time on average, the profile does not fit the charge boost cycles. Especially the region of the second charge boost step appears to behave significantly differently than expected. Mass is not removed from the main storage unit but rather augmented. This is the reverse process in comparison to what was anticipated and planed initially. A possible explanation could be that the recharge unit was wetter than the main storage unit because of the unfinished pre-conditioning step. However, this would not explain why the effect only appears during the second charge boost step and not the first one. Also, this behaviour was never observed in earlier experiments to that extent. Further discussion on this matter can be found in chapter 5.4.2.

The respective ΔX values for experiment 9 are depicted in Table 5-6.

Table 5-6: Comparison of two different approaches to compute the change in moisture content ΔX in %. The **theor. calc.** only uses the initial condition and then proceeds to calculate all other values purely on a theoretical basis using the Dubinin-Astakhov equation. The **T,p method** uses the experimental values of temperature and pressure along with the Dubinin-Astakhov equation to calculate ΔX.

Cycle index	ΔX theoretical calc. [%]	ΔX T,p calc. [%]
1	1,18	0,79
2	1,13	0,11
3	1,09	0,13
4	0,97	0,07
5	0,90	0,05
6	0,84	0,07

The results show that the experimental results for ΔX are significantly lower than the theoretically expected. A possible explanation for this behaviour could be the unfinished pre-conditioning process. This may have caused a lower initial pressure and moisture load within the main storage unit. These two effects lead to a lower pressure gradient between main storage unit and recharge unit and hence a lower mass transfer. The assumption of unfinished pre-conditioning is backed up the following facts:

- The missing temperature increase in the main storage unit during the recharge steps (almost no freed adsorption energy due to little to no water mass flow)

- A higher starting temperature in the main storage unit than usual

- The initial pressure of the main storage unit being too low (lower moisture content in the unit, $X_{initial} = 21,02$ % compared to the usual $X_{initial} = 27,8$ %)

5.3.4 Experiment 10

The pressure levels for all three vessels are depicted in Figure 5-20.
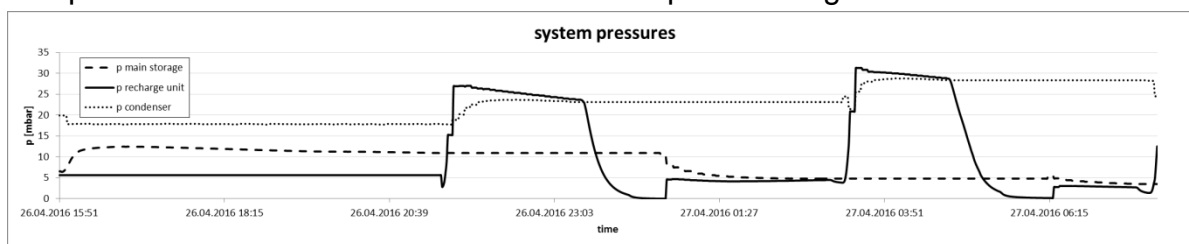
Figure 5-20: Pressure levels over the course of experiment 10 of all three vessels.

Experiment 10 showcases two problems that have already been encountered during earlier test runs. Firstly, the starting pressure of the main storage is too low, at 15 mbar instead of the anticipated 20. This may be the result of an unfinished pre-conditioning process as mentioned in the sub chapter experiment 9.

Secondly, the pressure increases again with each charge boost cycle (discussion see chapter 5.4.1). By counting the pressure peaks, the number of charge boost steps can be determined. It has to be mentioned that, for a similar time frame, experiment 10 only yields two of those steps, whereas experiment 7 and 9 resulted in 3 and 6 steps respectively.

The temperature levels of the main storage unit and recharge unit are depicted in Figure 5-21.

Figure 5-21: Temperature levels over the course of experiment 10 for main storage unit and recharge unit.

The temperature profile fulfils the theoretical predictions. Also the small temperature peaks during the charge boost step are present, contrary to experiment 9. The initial temperatures are slightly too high, although not as significantly as in experiment 9.

The masses of the main storage and the recharge unit are depicted in Figure 5-22 with two different axes.

Figure 5-22: Masses of the main storage unit and the recharge unit over the course of experiment 10 with two differently scaled axes (mass main storage left axis, mass recharge unit right axis).

The mass of the main storage shows an unexpected behaviour. It increases during the second charge boost step which is the opposite of the anticipated course. Also, the mass of the recharge unit shows different results than predicted. The peaks are not equal in mass but decrease as well. A possible explanation as well as a discussion regarding these observations can be found in chapter 5.4.2.

The respective ΔX values for experiment 10 are depicted in Table 5-7.

Table 5-7: Comparison of two different approaches to compute the change in moisture content ΔX in %. The **theor. calc.** only uses the initial condition and then proceeds to calculate all other values purely on a theoretical basis using the Dubinin-Astakhov equation. The **T,p method** uses the experimental values for temperature and pressure along with the Dubinin-Astakhov equation to calculate ΔX.

Cycle index	ΔX theoretical calc. [%]	ΔX T,p calc. [%]
1	1,18	2,69
2	1,13	1,04

The values show good correlation although the first experimental value is too high compared to the calculated one. This is a phenomenon which is already known from experiment 8.

5.4 Discussion of the obtained results

Before the obtained results are reviewed and compared, the problems encountered during the experiments shall be sorted and discussed.

5.4.1 Pressure

Regarding pressure, two different aspects have to be considered for the error evaluation. Firstly, as only one pressure sensor exists in the plant, the pressure measurement has to follow a special regime, which is explained in the following paragraph.

Each time the pressure in one unit needs to be determined, the respective vessel needs to be opened to the steam canal and all other units need to be closed off (description see chapter 4.1.319). This results in the steam canal having the same pressure as the respective unit. If the first unit is then closed off again and the pressure in a different vessel is measured, the pressure in the canal and the vessel reach equilibrium. This may result in a pressure drop or increase in the opened unit, depending on its state and the pressure in the canal. However, the adsorption or desorption of steam/water on the zeolite may compensate this effect, which makes an assessment of the influence on the experiments rather difficult.

Secondly, the pressure during the experiments repeatedly increased. An increase with each consecutive charge boost step was most commonly observed. During the experimental runs, possible reasons and countermeasures have been discussed with employees of AEE Intec. The final conclusion of this discussion was that inert gases enter the system over the course of the process and influence the pressure. This assumption is supported by the fact that the qualitative course of pressure profiles is actually fitting, merely the base pressure is too high. Also, the step-wise increase strengthens the idea of an increasing error source (leakage rate over time). However, it has to be mentioned that the pressure in experiment 8 decreased after an initial increase. This may be explained by the inert gases being adsorbed at the dried zeolite in the main storage unit. Additionally, the increase in pressure was observed during every experiment except for test run 9, although no structural changes were made. A possible explanation for this may be the long run time of the earlier experiment 8 and the aforementioned pressure decrease.

5.4.2 Mass

Considering the mass of the different vessels, a general remark concerning the scales has to be made. After finishing experiment 6, a malfunction of the main storage scale was discovered and the unit was exchanged for a different one. However, the assumption that it was a specific error of just one specific scale was proven wrong. An employee at AEE Intec, Reinhard Werner [32] investigated the case further after his experiments with the plant had shown the same problems with mass measurement as well. Contacting the scale manufacturer, it was determined that the used scales are not suited for long term mass measurements. If they are loaded for a longer period of time than suggested, the scale starts to "drift". This means that the mass measurement changes without the actual mass changing. The rate of change itself is arbitrary, as well as the direction of the drift (both in- and decrease have been observed). However, long term mass measurement was the intended purpose. As no other options were available, a rather pragmatic solution was chosen. The vessels are removed from the scales after measurement periods in order to relieve them before further use. A second discovery by Werner [32] was that the scales are equipped with a mass compensation program. This system compensates small changes in mass in order to deliver a stable signal even if the object is slightly moved. In the case of the testing plant, this effect is actively cancelling out the small mass changes that occur during the experiments.

Unfortunately, these discoveries were made after the initial experiments had been finished and could not be taken into account during the test runs. Therefore, all mass measurements have to be reviewed critically. Regarding the fluctuations and unexplainable in- or decreases in mass during the experimental runs, it can be stated that these effects are caused by the scales themselves. Also the calculations conducted in chapter 5.3.1, show that the values obtained from mass measurement do not correspond with the other measured or calculated values.

In conclusion, it can be stated that the mass measurement did not work as intended and cannot be the basis of a scientific assessment. Temperature and pressure measurements will be used for the evaluation of the experiments instead. For future works with the plant, new arrangements need to be made to provide accurate measurement technology.

5.4.3 Conclusion of the first round of experiments

In order to review whether the experiments could verify the aforementioned theoretical concept by Müller [30], the ΔX values of the respective experiments are compared. As mentioned in chapter 5.4.2, the values obtained from the mass measurements are not taken into account. Instead, the change in moisture content is determined by a calculation using the temperature and pressure levels as well as the theory of Dubinin-Astakhov [22]. Also, a purely theoretical calculation was conducted as a reference value. The collected data is depicted in Table 5-8.

Table 5-8: Summary of all ΔX values of experiments 7-10 (exp. 7 = experiment 7) in %. Purely theoretical values which have been calculated using the Dubinin-Astakhov equation are listed as a reference value as well.

Cycle index	ΔX exp. 7 [%]	ΔX exp. 8 [%]	ΔX exp. 9 [%]	ΔX exp. 10 [%]	ΔX theoretical calc. [%]
1	1,08	2,65	0,79	2,69	1,18
2	1,27	1,53	0,11	1,04	1,13
3	1,75	1,37	0,13		1,09
4		1,07	0,07		1,03
5		-0,09	0,05		0,97
6		0,09	0,07		0,90
7		0,42			0,84
8		-0,03			0,78
9		0,42			0,72
10		0,25			0,67
11		0,22			0,61
12		-0,05			0,56
13		-0,04			0,52
14		0,03			0,47
15		0,07			0,43
16		-0,01			0,39

In order to further assess the experimental data of the different experiments, not the ΔX values but rather the absolute X values will be plotted over the number of re-charge cycles. The resulting curves alongside the theoretical one are depicted in Fi-gure 5-23.
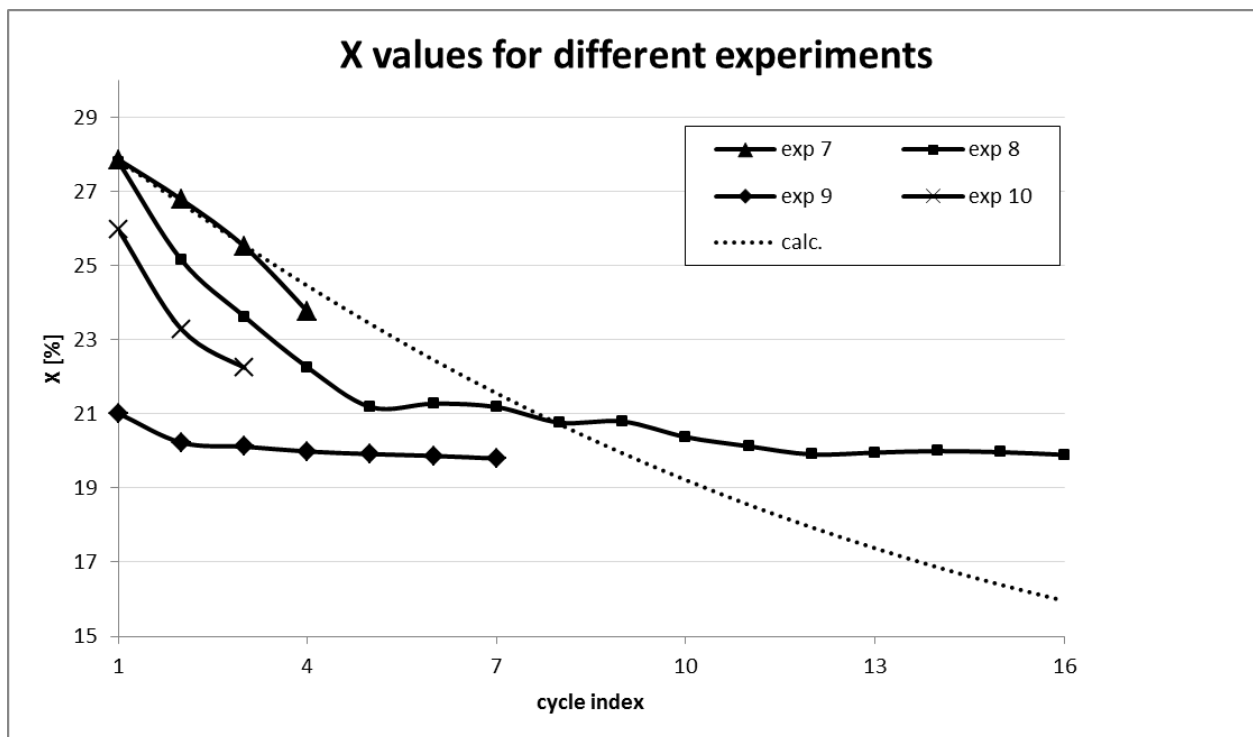
Figure 5-23: Plot of the respective ΔX values for all considered experiments as well as the purely theoretical model calculated with the Dubinin-Astakhov equation (dotted line).

The graphs are in adequate agreement with each other. The different starting points due to the unfinished pre-conditioning in experiment 9 and 10 can be seen as a dif-ference in the first point. The further course of the respective curves, however, is in good alignment with the rest of the data. It is apparent that the experiments reach a threshold after a certain number of recharge cycles. This was predicted by the theo-retical model, although the theoretical threshold is much lower and does not appear until approximately 30 recharge cycles. This deviation can be explained by the prob-lems with the system pressure. A higher pressure in the plant reduces the effective-ness of the process by raising the threshold to higher moisture content levels.

Overall, the experiments can be labelled a success. They show that the charge boost process is indeed a viable option to further reduce the moisture content in a seasonal thermal energy storage system, thereby raising its state of charge. To show the practical significance of this process, the SOC for pure desorption at 60 °C is compared to the threshold value in the main storage obtained in experiment 8 with charge boost technology. The results are shown in Figure 5-24.
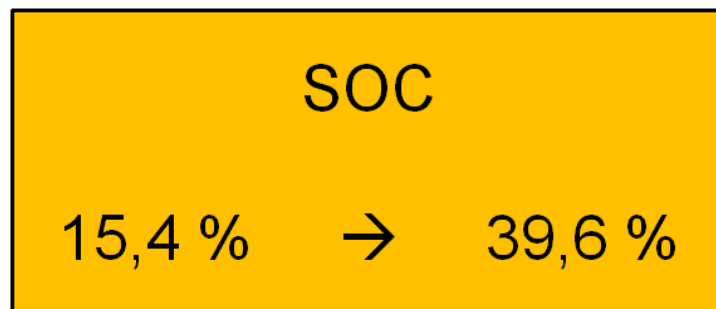
Figure 5-24: Possible improvement in SOC by using charge boost technology instead of normal desorption. The high temperature level of the main storage unit was at 60 °C whereas the recharge unit had a high temperature level of 140 °C.

For further experiments, it could be promising to vary the temperature levels of the respective units in order to reach even better results. Compared to the COMTES project [24] [25] carried out at AEE Intec, which already used the charge boost technology, the following insights could be obtained concerning the charge boost technology:

- The charge boost technology also works for several consecutive cycles, depending on the size ratio of the main storage and recharge unit and the respective temperature levels.

- Different sizes can be beneficial to the process. (During the COMTES project, units of the same size have been used for the charge boost technology.)

- With the charge boost technology, desired SOCs can be reached by using comparably lower temperatures than with normal desorption. This is beneficial to the process as the efficiency of solar thermal collectors is higher at lower temperatures. Also, the possible lower temperature levels make this process attractive for use in periods of transition or even during winter. These effects are the main motivation for the development of a new charge boost concept, as presented in the following chapters.

6 Development of new concepts with regard to the charge boost technology

The main benefit of the charge boost technology is the possibility to use comparably low temperatures to further charge a unit that has already been charged by normal desorption [29]. Taking the additional insights listed in chapter 5.4.3 into account, a new concept for the use of the charge boost technology during winter should be developed. During this time, partially charged main storages are present along with large quantities of solar radiation energy at low temperature levels. Recharging these units in winter would be beneficial to the cycle efficiency by raising the number of cycles performed each year. Additionally, the amount of adsorption material needed to operate a seasonal thermal energy storage system would decrease, thereby reducing the cost and also the space demand of the whole apparatus. However, such a concept would only be viable if it can compete with classic short term storage system such as hot water tanks. Therefore, a comparison of the new concepts with reference systems is required as well. The design of such a concept for recharge in winter is structured in different subtasks. These tasks have been carried out consecutively by the author and are listed in the following:

- Definition of the system properties

- Material screening for the recharge unit and selection of the most promising system

- Theoretical predictions of the energy efficiency in winter and optimization of the system

- Comparison of the finished design with reference systems

6.1 Definition of the system properties

In order to design the new concept, system boundaries and properties have to be chosen first. The time period for which the system should be developed is defined as the 1st of December to the 28th of February. Also, the simulated house has to be defined. The characterization of the building follows the template used in the Tes4Set project except for the collector area and is given in Table 6-1.

Table 6-1: Characteristics of the simulated house for the development of the new charge boost concept for winter.

single family house in Graz	
surface area	150 m²
space heating demand	15 kWh/m² per year
domestic hot water demand	200 l/d (45 °C)
collector type	vacuum tube collectors[8]
collector area	30 m²

The respective data for solar radiation including collector efficiency was provided by Alexander Goritschnig and simulated by Dagmar Jähnig (full data can be retrieved from AEE Intec, referring to IEA SHC task 26 [33] and task 32 [34]). After the house/consumer is defined, the temperature levels of the system have to be stated.

5 °C is chosen for the minimum temperature. This value was selected because of the condition that it should be constantly available during winter. Although an even lower temperature would be beneficial to the process, it has to be considered that the hydraulics of the system and the adsorption itself operates with water, which excludes temperatures of 0 °C and below. The value of the high temperature benchmark in the system was defined differently. As a first step, the available solar radiation of different temperature levels in the respective months is determined.

---

[8] The parameters of the chosen collector can be found in the appendix.

Lower temperatures result in higher collector efficiency and can therefore provide more energy to the system. A comparison of power provided by the collectors for different temperature levels in the months of December, January and February and a collector area of 30 m² is depicted in Figure 6-1.
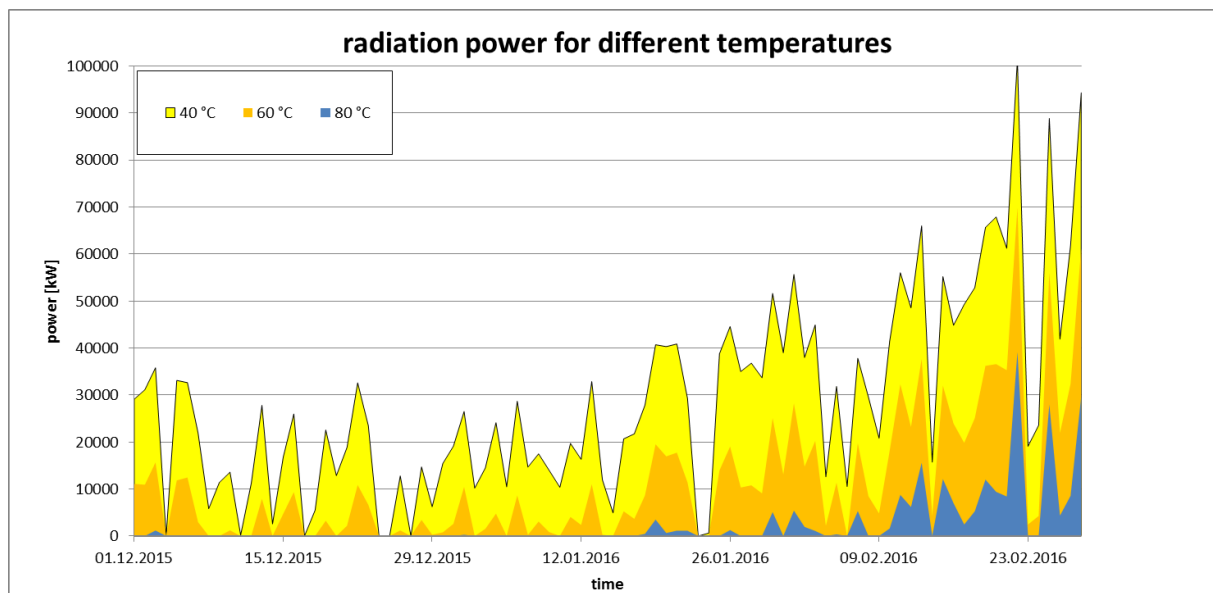
Figure 6-1: Comparison of power provided by the collectors for different temperature levels in the months of December, January and February and a collector area of 30 m².

As explained earlier, the lower the temperature is the more power can be provided to the process. As for the discussed system properties, two temperatures, 40 °C and 60 °C, have been chosen as maximum for further evaluation. For the rest of the calculations, the radiation data will be multiplied with a cycle efficiency factor of $F_c=0,7$ which sums up all losses and efficiency factors in the virtual system. A summary of temperature levels for the different vessels and process steps is given in Table 6-2.

Table 6-2: Summary of temperature levels for the different vessels and process steps for the newly developed concept.

process step	temperature [°C]
temperature main storage	40 °C/60 °C
temperature recharge unit (desorption)	40 °C/60 °C
temperature recharge unit (charge boost)	5 °C
temperature condenser	5 °C

6.2 Material screening for the recharge unit

As the frequently changing and generally low temperatures in the recharge unit do not favour zeolite as adsorption material, a material screening is performed, especially concerning silica gels. The reason silica gels are more suited for this process than zeolite 13XBF is evident by the differently shaped isosteric curves of both materials. In Figure 6-2, the isosteric curve for zeolite and a silica gel (Sorbead R) are depicted with a rectangle marking the operating range for the considered system.
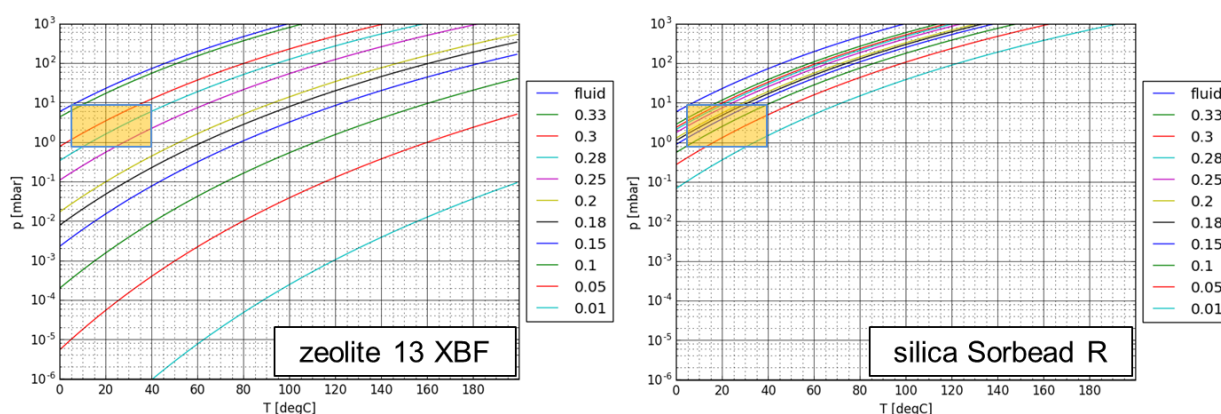
Figure 6-2: Isosteric curves for zeolite 13XBF **(left)** and silica gel Sorbead R **(right)** with rectangles marking the operating range for the considered system.

While inspecting the operating range, it becomes apparent that the isosteric lines are much more tightly packed for silica gel than for zeolite. This means that, with the same pressure gradient, more water can be ad-/desorbed per kg silica gel than per kg zeolite in that region. However, the long term storage efficiency is comparably low for silica gels. Therefore, the regarded system will consist of a zeolite filled main storage (good long term storage capabilities) while the recharge unit will be most likely equipped with a different adsorption material (good cycle efficiency in the desired temperature and pressure range). In order to determine which material suits the requirements best, theoretical calculations are performed. Six different materials are investigated. The list is depicted in Table 6-3 (component data see appendix).

Table 6-3: List of all 6 investigated materials for the material screening.

Name	Type
Fuji Silysia Ltd – Type 3A	silica gel
Fuji Silysia Ltd – Type RD	silica gel
BASF SE – Sorbead R	silica gel
Sylobead SGB 127	silica gel
13XBF	zeolite
AQSOA Z02	SAPO-34

The further material screening is structured as follows:

a) Design and dimensioning of the recharge unit

b) Calculation of the dimensions for the respective main storages

c) Calculation of three consecutive charge boost steps and evaluation

These three steps are carried out for all six materials and the two system temperatures 40 °C and 60 °C. Either a constant main storage temperature or a variable main storage temperature will be considered for the system. A constant main storage temperature provides better performance of the system while also requiring heating energy to supply the desorption energy during the charge boost steps. This energy demand is not present for a variable main storage temperature as the system is designed in a way in which the sensible heat of the main storage is used to provide the desorption energy (hence the heat loss of the system over the course of the process). However, the decrease in main storage temperature worsens the efficiency of the charge boost process. These variations add up to 6 x 2 x 2 = 24 calculations, which have to be performed. In the following chapters, the calculations will be explained in general and the finished results will be presented.

6.2.1 Design of the recharge unit

The recharge unit is designed in a way, which enables the charge boost process to be performed at least every fourth day in the defined winter months. The list of energy per day is sorted by the respective amount of available energy. Then the minimum value of the top 25% is chosen as the design specification for the system. The results are depicted in Table 6-4.

Table 6-4: Minimum values for every fourth day in winter for 40 °C and 60 °C.

minimum value provided every fourth day for 40 °C	39956,4 kJ/d
minimum value provided every fourth day for 60 °C	17533,8 kJ/d

In the next step the mass of the recharge units for each material is defined in a way, which enables a full desorption of the unit with the respective quartile value (full desorption means the furthest possible desorption under process conditions). These calculations are performed by using the theory of Dubinin-Astakhov [22]. As several mathematical formulas will be mentioned in this chapter, a summary of the most important ones is provided at this point.

Moisture content Dubinin-Astakhov

$$X(T,p) = X_{max}(T) * exp\left[\left(-\frac{RT}{EM} * ln\left(\frac{p_S(T)}{p}\right)\right)^n\right] \tag{6.1}$$

Maximum moisture content Dubinin-Astakhov

$$X_{max}(T) = W_0 * \rho(T) \tag{6.2}$$

Pressure Dubinin-Astakhov

$$p(T,p) = p_S(T) * exp\left[\frac{EM}{RT} * \left(ln\left(\frac{X}{X_{max}(T)}\right)\right)^{\frac{1}{n}}\right] \tag{6.3}$$

Saturation vapour pressure Antoine

$$p_S(T) = \exp\left(A - \frac{B}{C+T}\right) \tag{6.4}$$

Water mass Balance between main storage and recharge unit

$$m_{MS} * \left(X_{start}(T,P) - X_{end}(T,P)\right) - m_{REC} * \left(X_{end}(T,P) - X_{start}(T,P)\right) = 0 \tag{6.5}$$

Formula for sensible heat in adsorption material

$$\Delta Q = \Delta T * m_{ads} * (cp_{water} * \Delta X + cp_{ads}) \tag{6.6}$$

For the dimensioning of the recharge unit, the amount of energy necessary for the full desorption of 1 kg material is determined. This is done by firstly computing the maximum possible change in moisture load ΔX for 40 °C/60 °C with a condensation temperature of 5 °C. Afterwards, this ΔX value is divided by the maximum possible ΔX of the material. This %-value of the maximum desorption potential is then multiplied with the maximum adsorption energy as depicted in equation 6.7 for 40 °C (adsorption energy obtained from Kohl [35], values in the appendix).

$$\frac{\Delta X_{40°C}}{\Delta X_{max}}[\%] * Q_{ads}\left[\frac{Wh}{kg_{material}}\right] = Q_{ads40°C}\left[\frac{Wh}{kg_{material}}\right] \tag{6.7}$$

After this value has successfully been calculated, the following division provides the amount of adsorption material that can be fully desorbed during a quarter of all winter days.

$$\frac{Q_{solar\_daily}[Wh]}{Q_{ads40°C}\left[\frac{Wh}{kg_{material}}\right]} = kg \ material \ in \ the \ recharge \ unit \tag{6.8}$$

The results for all six materials and the two system maximum temperatures are given in Table 6-5.

Table 6-5: Results for the masses of the recharge units for the 40 °C and 60 °C system and every material.

Material	mass 40 °C [kg]	mass 60 °C [kg]
Fuji Silysia Ltd – Type 3A	40,84	15,20
Fuji Silysia Ltd – Type RD	35,77	13,47
BASF SE – Sorbead R	41,78	15,00
Sylobead SGB 127	40,65	15,07
13XBF	254,94	53,06
AQSOA Z02	91,88	18,19

It is apparent that the results for the four silica gels are almost identical while the SAPO-34 AQSOA Z02 and especially the zeolite 13XBF behave differently. The large required mass of the zeolite 13XBF shows how strong the influence of the different adsorption behaviours is. For the given temperature levels, about 5 times more zeolite is needed to store the same amount of energy as silica gels.

6.2.2 Calculation of the dimensions for the respective main storages

With the masses of the respective recharge units from Table 6-5, the masses of the main storages can be determined via iterative calculation carried out in Excel. In order to perform this calculation, the assumption is made that the main storage has a starting moisture content of $X_{MS\,start} = 30\%$. The dimension of the main storage is governed by the requirement that it should provide enough water to fully adsorb the recharge unit at equilibrium during the charge boost step. This is done by an iterative calculation, using the Excel solver. The schema for the calculation steps is depicted in Figure 6-2.
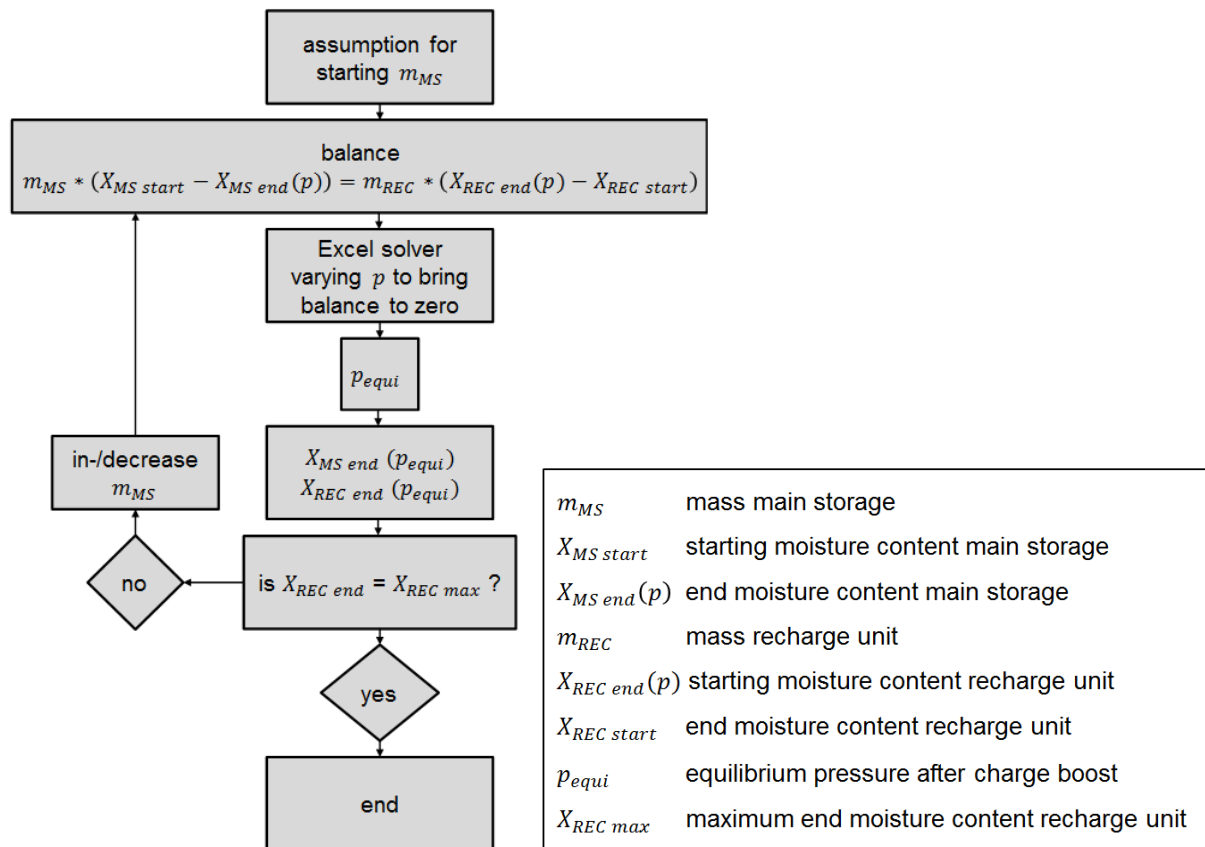
Figure 6-3: Flowsheet for the iterative calculation of the main storage masses for constant main storage temperature.

However, this calculation is only that simple for the case of constant main storage temperature. As the temperature varies in the second case, additional calculations have to be performed. Not only the Excel solver add-in but also macros are being used to determine the main storage masses with Excel (Excel sheet available at AEE Intec). A simple flow sheet of the calculation process is shown in Figure 6-2.
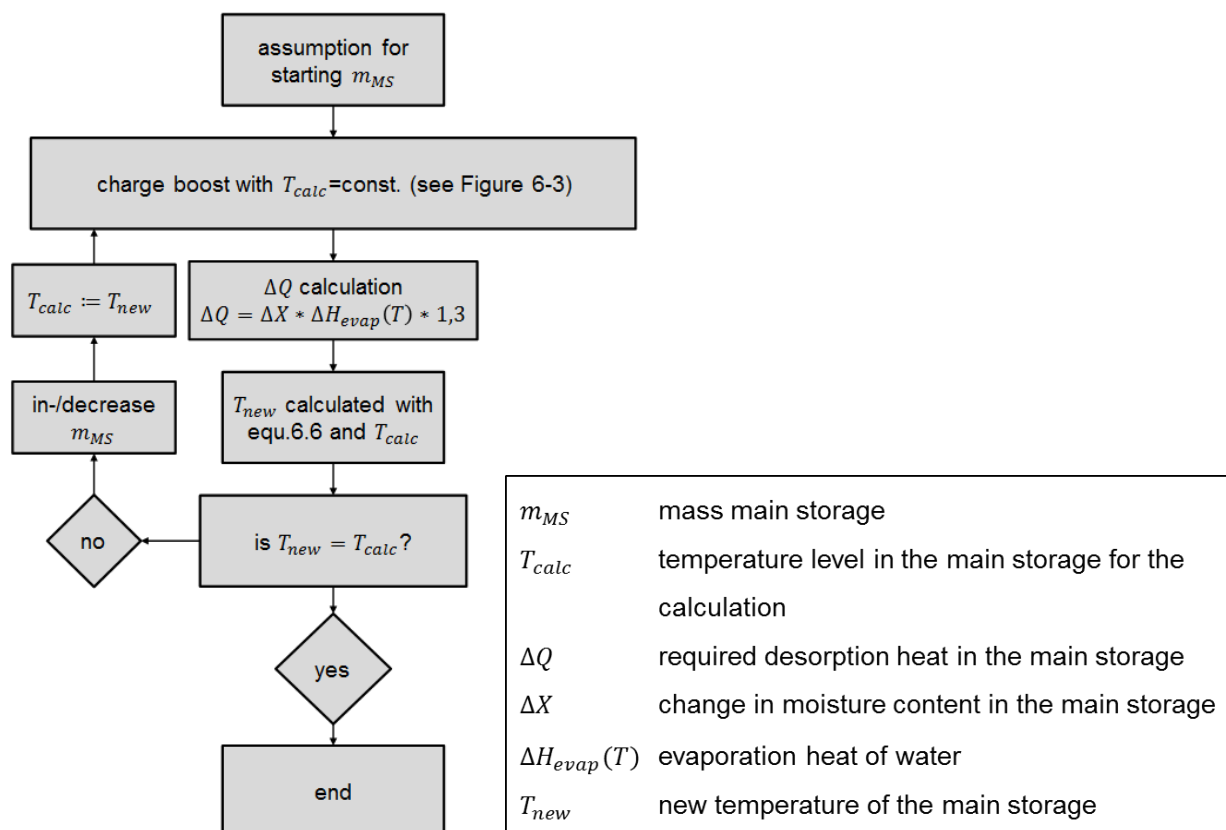
Figure 6-4: Flowsheet for the iterative calculation of the main storage masses for variable main storage temperature.

After these 24 calculations are completed, four sets of combined main storage and recharge unit sizes are generated. The data is given in Table 6-9Table 6-6, Table 6-7, Table 6-8 and Table 6-9

Table 6-6: Main storage and recharge unit masses for all six components for **40 °C** and **constant** main storage temperature.

Material	mass main storage [kg]	mass recharge unit [kg]
Fuji Silysia Ltd – Type 3A	730	40,84
Fuji Silysia Ltd – Type RD	750	35,77
BASF SE – Sorbead R	850	41,78
Sylobead SGB 127	780	40,65
13XBF	310	254,94
AQSOA Z02	400	91,88

Table 6-7: Main storage and recharge unit masses for all six components for **40 °C** and **variable** main storage temperature.

Material	mass main storage [kg]	mass recharge unit [kg]
Fuji Silysia Ltd – Type 3A	2283	40,84
Fuji Silysia Ltd – Type RD	2301	35,77
BASF SE – Sorbead R	2620	41,78
Sylobead SGB 127	2404	40,65
13XBF	1023	254,94
AQSOA Z02	1268	91,88

Table 6-8: Main storage and recharge unit masses for all six components for **60 °C** and **constant** main storage temperature.

Material	mass main storage [kg]	mass recharge unit [kg]
Fuji Silysia Ltd – Type 3A	97	15,20
Fuji Silysia Ltd – Type RD	93	13,47
BASF SE – Sorbead R	109	15,00
Sylobead SGB 127	96	15,07
13XBF	55	53,06
AQSOA Z02	68	18,19

Table 6-9: Main storage and recharge unit masses for all six components for **60 °C** and **variable** main storage temperature.

Material	mass main storage [kg]	mass recharge unit [kg]
Fuji Silysia Ltd – Type 3A	314	15,20
Fuji Silysia Ltd – Type RD	301	13,47
BASF SE – Sorbead R	354	15,00
Sylobead SGB 127	312	15,07
13XBF	181	53,06
AQSOA Z02	227	18,19

6.2.3 Calculation of three consecutive charge boost steps

In order to compare the efficiency of the different systems, three consecutive charge boost steps have been calculated for every setup. These calculations have been carried out using the same equations as depicted in Figure 6-3 and Figure 6-4. This time the masses of the two units are of course fixed values and therefore the loop for the iterative calculation of the main storage mass does not need to be executed for the case of constant main storage temperature. However, for the system with changing main storage temperature, the loop for the determination of the end temperature is still needed, hence only the changing of the unit mass can be left out. The end conditions of each first step are then used as starting conditions for the second step (temperature, pressure, moisture load). The criteria for evaluation will be the Δm of water for the system pairings. A larger amount of moved water results in a higher increase of the SOC of the main storage. The results for all four system setups (40 °C and 60 °C for T=const. and T=variable respectively) are shown in Figure 6-5, Figure 6-6, Figure 6-7 and Figure 6-8.
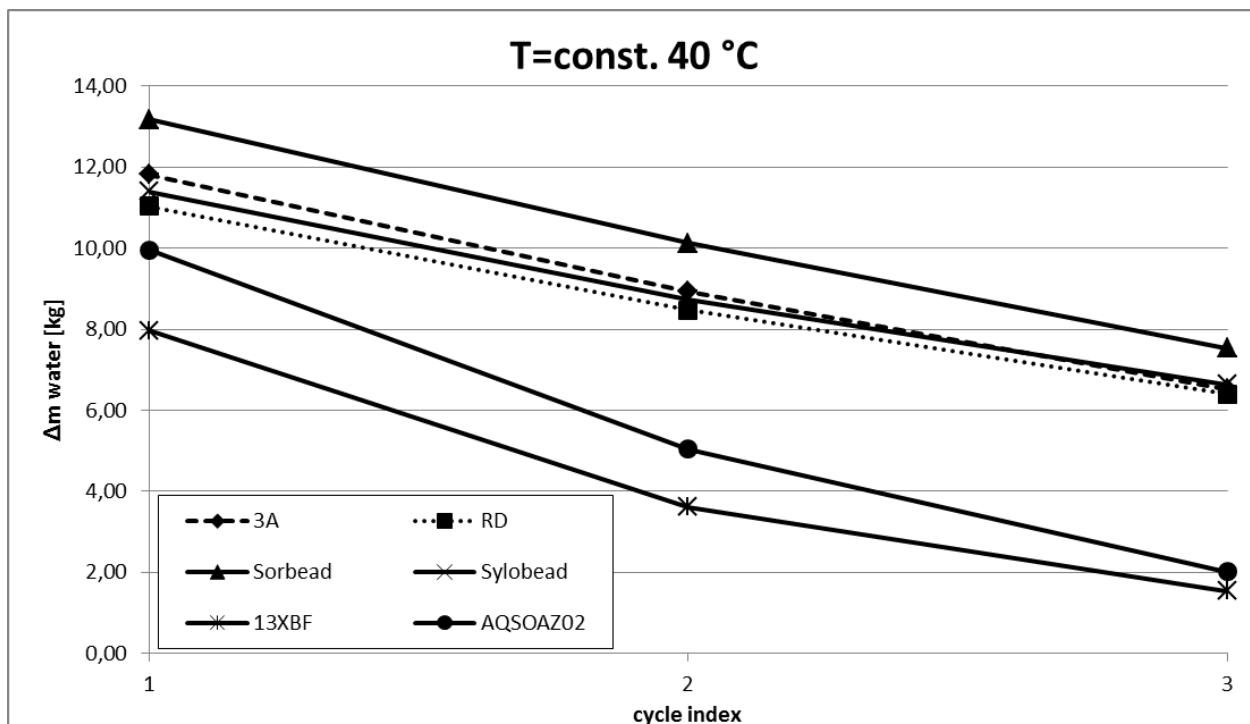
Figure 6-5: Amount of moved water Δm for all six components for 40 °C and constant main storage temperature.
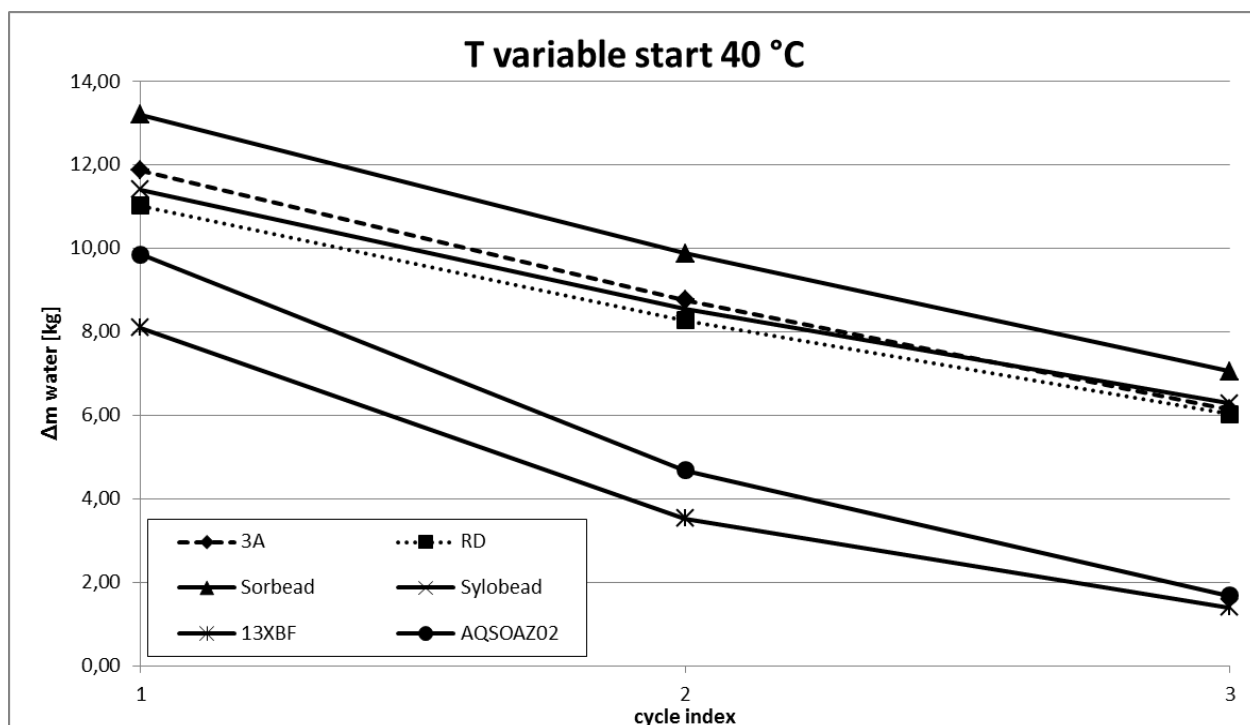
Figure 6-6: Amount of moved water Δm for all six components for 40 °C and variable main storage temperature.
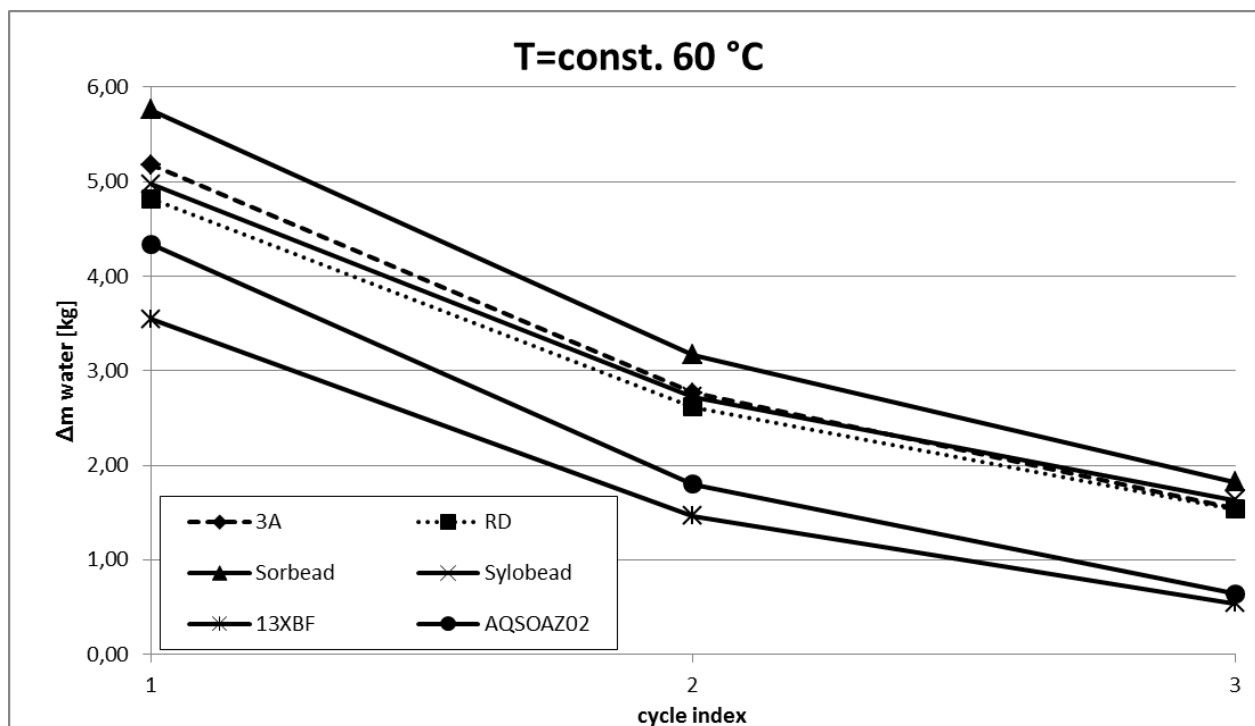
Figure 6-7: Amount of moved water Δm for all six components for 60 °C and constant main storage temperature.
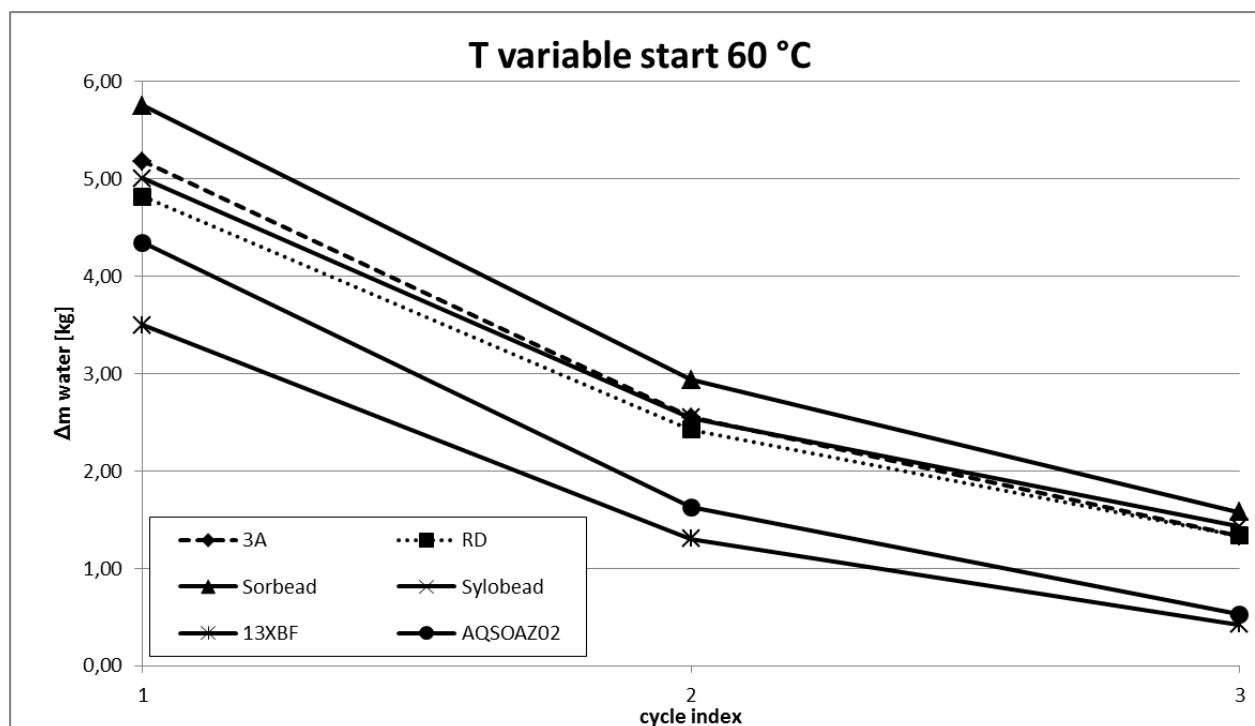
Figure 6-8: Amount of moved water Δm for all six components for 60 °C and variable main storage temperature.

It is apparent that nearly the same courses can be observed for constant and variable temperatures alike. This is no coincidence but it is caused by the fact that the main storage and recharge unit have been designed in a way, which enables the first charge boost step to fully adsorb the recharge unit. Since the amount of adsorbent is only determined by the solar energy at the respective temperatures, the units have the same size for constant and variable main storage temperature (for 40 °C and 60 °C). Regarding the calculations with variable main storage temperature, the loss in temperature for each material pairing is depicted in Figure 6-9 for 40 °C and Figure 6-10 for 60 °C respectively. The calculation of the temperature loss has been validated by a second calculation performed with a python script by Georg Engel (private communication).
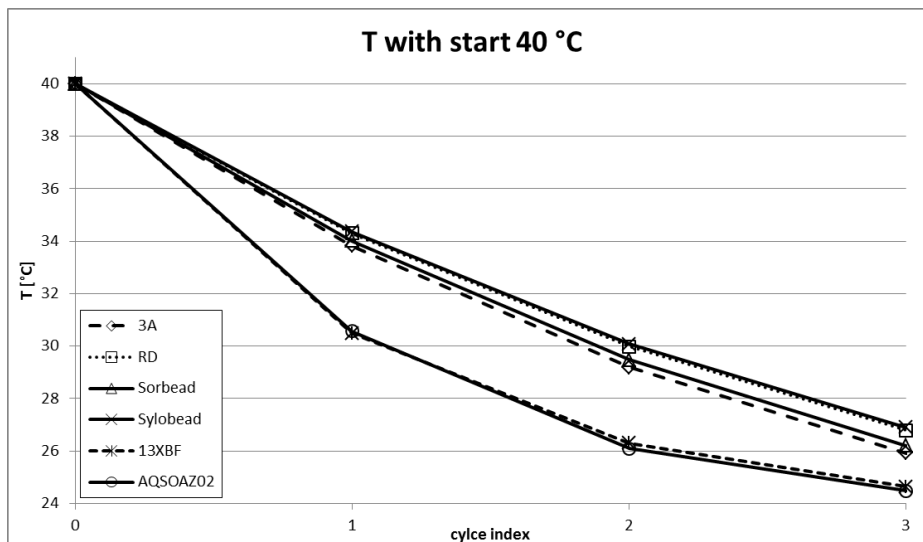
Figure 6-9: Loss in temperature for each material pairing with a starting temperature of 40 °C for three charge boost cycles.
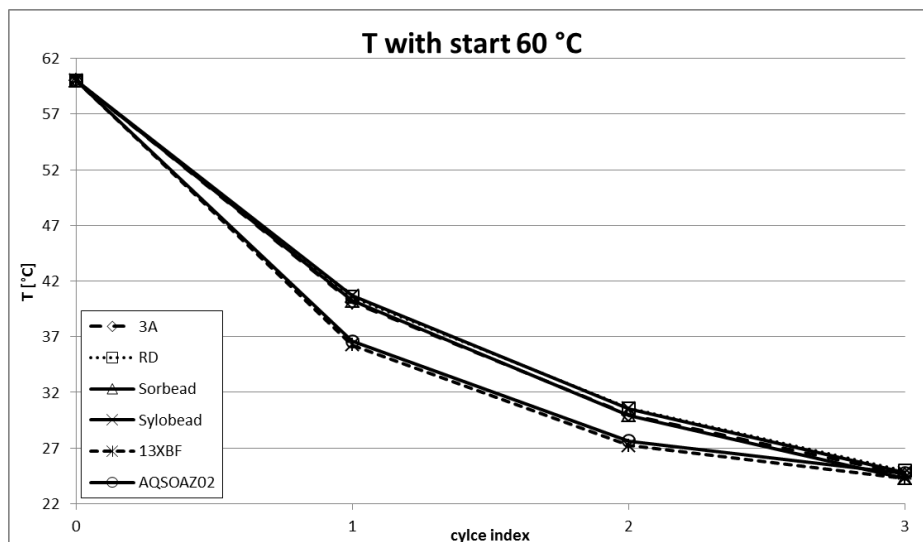
Figure 6-10: Loss in temperature for each material pairing with a starting temperature of 60 °C for three charge boost cycles.

Out of all the material pairings, the setup with the most amount of moved water, hence the most effective one was the Sorbead R system, in each of the four categories respectively. Additionally, out of all four setups, the one with a desorption temperature of 40 °C and constant main storage temperature appeared to be the most promising candidate as the amount of moved water is the highest (see Figure 6-12). Therefore, this system was selected for all further considerations.
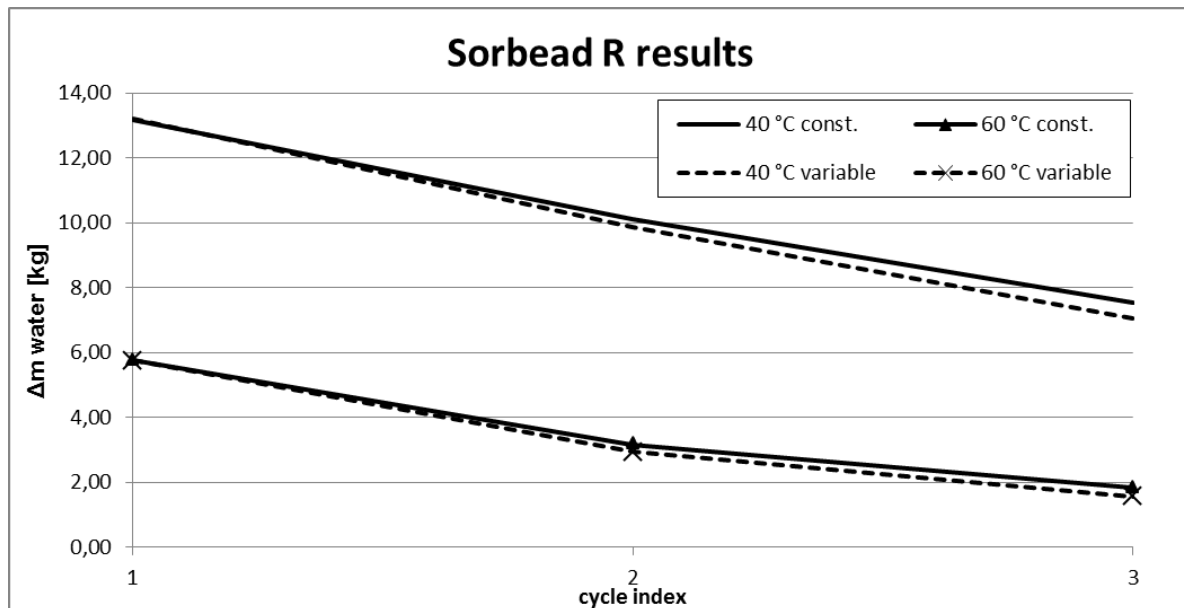
Figure 6-12: Comparison of the mass of moved water Δm for all four system setups for the most promising material Sorbead R.

In order to better depict the operating range of the new concept with Sorbead R, the absolute moisture load of the main storage unit (for T=40 °C and constant) throughout the process is depicted in Figure 6-11 as well.
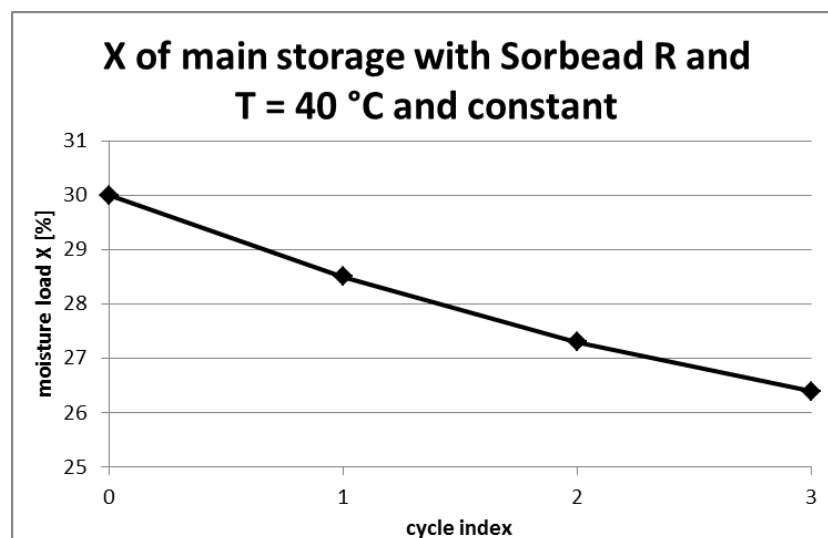
Figure 6-11: Moisture load X of the main storage unit with Sorbead R and T= 40°C and constant.

6.3 Theoretical predictions of the energy efficiency in winter

In order to fully assess the amount of energy the system can store, an operation block procedure is implemented. Different "operation blocks" are designed, each with its specific energy demand. As the daily radiation energy for each day of the winter period is known, only a limited amount of tasks can be performed each day. Under the restriction that all charge boost steps must have a fitting desorption step of the recharge unit to form a pair, each day is filled with operation blocks. From the number of completed charge boost processes (one charge boost and one desorption step necessary), the amount of stored energy can be computed.

As stated in chapter 6.1, the system was designed in a way, which would make full desorption of the recharge unit possible for one in four days. However, this was only a first assessment to calculate the optimal mass ratio. It is apparent that for a higher number of smaller units, the flexibility of the system regarding the daily available energy increases drastically. Therefore, the original dimensions are abandoned, and only the known mass ratio (mass main storage to mass recharge unit ≈ 20:1) is used in further calculations. In order to investigate which case is the most promising one, the operation block system is carried out for five systems with different masses (they will be referred to only by the mass of the main storage unit from this point on). The respective masses of these five systems are displayed in Table 6-10.

Table 6-10: Main storage and recharge unit mass for the respective systems.

Mass main storage [kg]	Mass recharge unit [kg]
100	5
200	10
300	14,5
400	19,5
500	24,5

For all five systems, twelve operation blocks are defined. They are composed of desorption (desorp.) and charge boost (chargeb.) steps. Furthermore, they are labelled depending on the respective process step being carried out (first desorption in a cycle = desorp. 1, second charge boost in a cycle = chargeb. 2 and so on). They are displayed in Table 6-11.

Table 6-11: Operation blocks for the system. desorp. = desorption step, chargeb. = charge boost step, (1) first step in the three cycle process, (2) second step in the three cycle process, (3) third step in the three cycle process. They are sorted after appeal to be carried out.

Index	Type	Index	Type
1	chargeb. 1, chargeb. 2, chargeb. 3	7	chargeb. 1
2	chargeb.1, chargeb. 2	8	chargeb. 2
3	3 x desorp. 1	9	chargeb. 3
4	2 x desorp.1	10	desorp. 1
5	desorp.1, desorp. 3	11	desorp. 2
6	desorp. 1, chargeb. 1	12	desorp. 3

The index illustrates the level of attractiveness to carry out the respective block, e.g. operation block 1 is the most desirable one because three charge boost steps can be carried consecutively with only one instant of sensible heating up of the main storage unit. After all days of the winter period have been "filled" with operation blocks, the number of required single units is determined by examining the single days. If for example during one day, desorption step 1 is carried out three times, three single recharge units are required to do this. Combining this unit number with the scale of the different cases, the dimensions of the system can be determined. An overview of the results is depicted in Table 6-12, concerning the energy efficiency of the systems.

Table 6-12: Results for the operation block method for all five systems.

System	Stored energy	Efficiency[9]	Number of units	Total storage mass
[-]	[MJ]	[%]	[-]	[kg]
100 kg MS	880	48,76	4	400
200 kg MS	830	45,97	3	600
300 kg MS	740	40,93	2	600
400 kg MS	640	35,57	1	400
500 kg MS	625	34,52	1	500

6.4 Comparison of the final design with reference systems

The final results of the theoretical calculations are compared with two different kinds of energy storages.

- System one is a pure sorption thermal energy storage system with the same mass as the respective charge boost setup.

- System two is a conventional sensible hot water storage. As for all sensible storages, a temperature gradient is needed to discharge the system. Taking the high temperature level of 40 °C from the charge boost system as a reference, this results in a hot water storage temperature of 60 °C. The storage is dimensioned in a way that it can store the sum of solar energy available at the two strongest days at a temperature level of 60 °C. For operation, it is assumed that the system can store all available energy throughout winter as it is charged and discharged alternately.

---

[9] The efficiency was calculated as the ratio of stored energy compared to the total available solar radiation energy in winter. $\eta_{system} = \dfrac{Q_{stored}}{Q_{solar\_winter}} \, [\%]$

The three systems are compared regarding their energy storage intake during the winter period in [kJ]. The results are display in Table 6-13.

Table 6-13: Comparison of the theoretical results for the new concept with calculations for reference systems (pure desorption and hot water storage).

System	Charge boost [kJ]	Pure desorption [kJ]	Water storage [kJ]
100 kg	880	110	723
200 kg	830	129	
300 kg	740	129	
400 kg	640	110	
500 kg	625	111	

It can be stated that the recharge process does indeed seem to be able to match, if not exceed the short term storage capabilities of a hot water storage and especially of pure sorption systems in theory. A significant benefit in comparison to the hot water storage is the smaller volume of the system, with the hot water storage at about 0,8 m³ and the 100 kg recharge system with four separate units at 0,28 m³ in total. It has to be mentioned though that the low temperature heat source for the evaporation of the water is provided by a cost free source, as for example geothermal heat.

The main advantage of the charge boost system in comparison to the other two set-ups is that it can work with lower temperatures. This means that the collectors have a higher efficiency and can provide more energy to the system. Additionally, a lower temperature level leads to less sensible heat loss due to the heating up processes of the units. In order to validate the theoretical models, experiments are conducted at AEE Intec. Three consecutive charge boost steps should be carried out and compared to the theoretical results.

7 Adapting the experimental plant

In order to validate the theoretical calculations, experiments with the already described testing plant should be conducted. As another Master student [32] worked with the apparatus in the time period of the calculations, changes have been made to the plant.

The most significant change is the implementation of four new heating bands. This allows for a more even temperature profile in the main storage and recharge unit as each heating band can be controlled individually to match the requirements the plant imposes. Additionally, an adapted automatic process control system has been implemented. Not all operating modes of this automatic process control system have been used in the experiments presented in chapter 8. Therefore, only the relevant modes are described as all additional ones have been deactivated for the course of the author's experiments. An overview of the adapted process control system is depicted in

Figure 7-1.
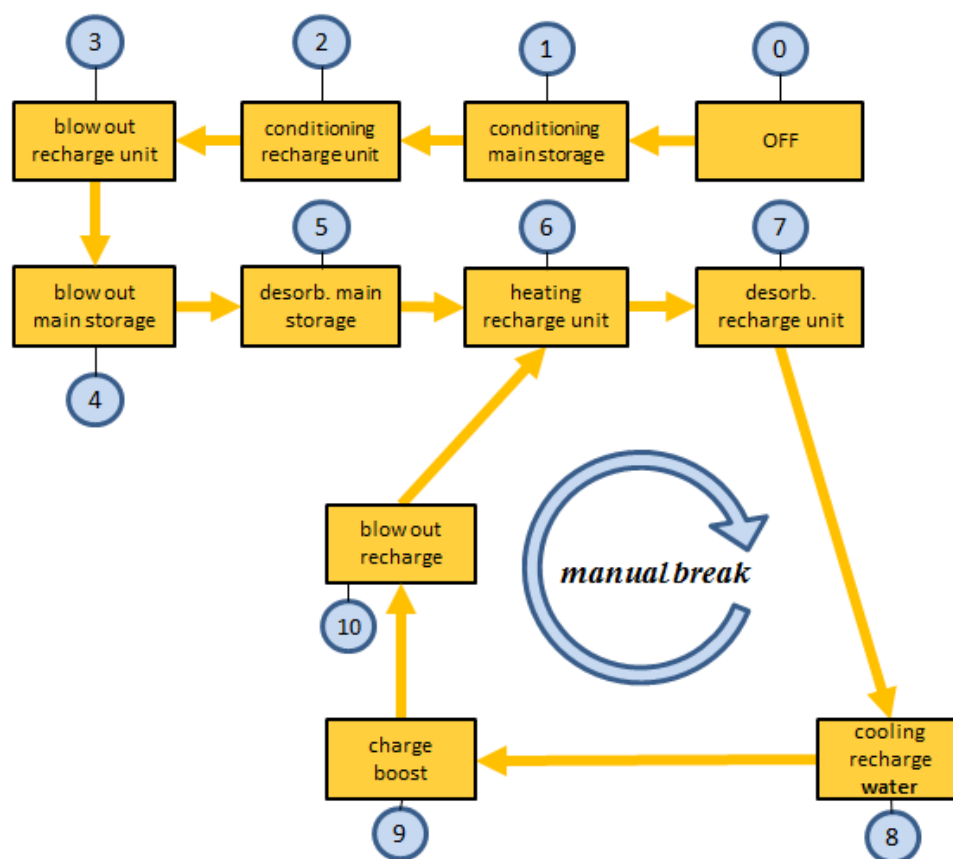
Figure 7-1: Schematic overview of the adapted process control system.

The new operating modes are 1 and 2, with mode 6 essentially being "regeneration recharge unit". Mode 1 and 2 are implemented to ensure the same initial conditions for each experiment.

As the desired material in the recharge unit has changed due to the results of the calculations, structural changes need to be made to the plant as well. The recharge unit is opened and the zeolite 13XBF is removed. Then, the vessel is filled with 655 g Sorbead R, the most promising material according to the calculations. The mass of Sorbead R is chosen so that the mass ratio equals the optimal mass ratio of 20:1 which was determined during the calculations. Due to the lower filling mass and hence smaller volume, the upper third of the recharge unit is not filled with sorption material. However, this should not influence the measurement in any way as this effectively only causes the steam canal to be slightly longer. The experimental procedure is the same as described in chapter 5.1, with the addition of the pre-conditioning steps. The manual break will be used after three consecutive charge boost cycles as this was also the number of cycles which was investigated during the calculations.

It has to be stated at this point that the cooling system at AEE Intec can only provide 6 °C as coldest temperature. Combined with the heat exchanger and tubing losses, this resulted in a low level temperature of 10 °C for the experiments instead of the 5 °C from the calculations.

8   Experimental findings and evaluation

In order to provide a fitting theoretical basis for the experiments at 10 °C, additional calculations for the Sorbead R system with T= 40 °C/constant have been carried out, using 10 °C as heat sink temperature level. The calculations are the same as described in chapter 6.2, with the difference that the mass ratio of main storage and recharge unit is not iterated again. It has to remain the same as in the already built experimental setup in order to be comparable.

Three experiments have been carried out to validate the theoretical model. A summary of the results for the change in moisture content in the main storage unit compared to the theoretical values is depicted in Table 8-1 (determined with the T,p method, see chapter 5.3.1).

Table 8-1: Summary of the change of moisture content in the main storage of each cycle and every respective experiment.

Cycle index	ΔX experiment 1	ΔX experiment 2	ΔX experiment 3	ΔX theoretical calculation
1	0,90	1,19	0,73	1,3
2	0,89	0,89	0,94	0,9
3	0,57	0,54	0,54	0,7

Also, the absolute moisture content values for all experiments (determined with the T,p method, see chapter 5.3.1) as well as the theoretical model are depicted in Figure 8-1.
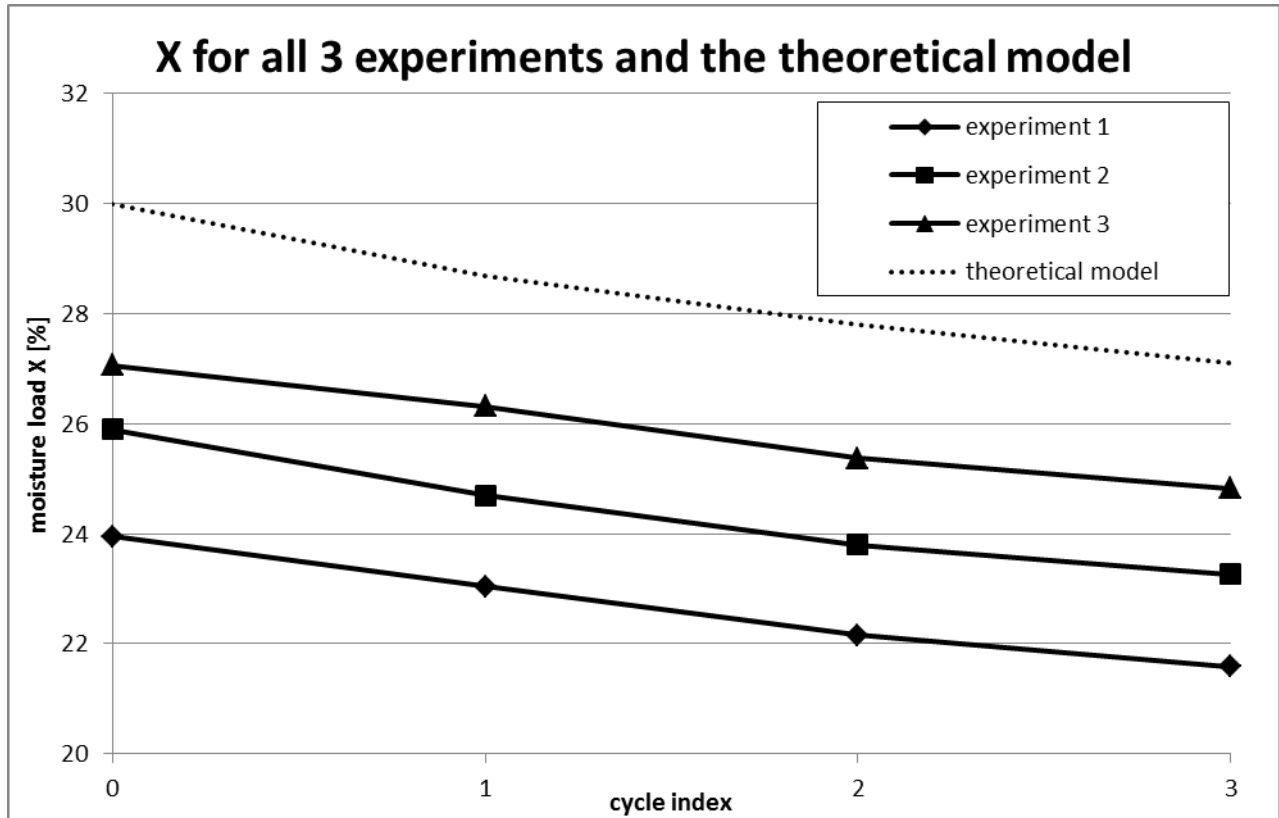
Figure 8-1: Absolute moisture content values in the main storage unit for all experiments (determined with the T,p method from the experimental data) as well as the values for the theoretical model.

From the obtained data it is apparent that the experimental results show worse charge boost properties than the theoretical model which was expected. The deviation between the three experiments may be caused by inert gases accumulating in the plant over the course of the test runs. As explained in chapter 5.4.1 this reduces the efficiency of the system. Especially for the charge boost process this is problematic, as the operation range is at a very low pressure level. Table 8-2 shows the inert gas pressure10 in the system at the end of all three experimental runs respectively.

_____

[10] The inert gas pressure is calculated based on the difference between the system pressure and the expected saturation vapour pressure of the condenser.

Table 8-2: Inert gas pressures in the system at the end of all three experiments respectively in mbar.

inert gas pressure exp. 1 [mbar]	inert gas pressure exp. 2 [mbar]	inert gas pressure exp. 3 [mbar]
23,26	25,40	26,10

Also, it has to be noted that the starting conditions of the three respective experiments differ from the theoretically defined ones (see point 0 in Figure 8-1). This has been caused by a malfunctioning of the pre-conditioning process.

Nevertheless it can be stated that the charge boost technology indeed provides a possibility to further dry main storages in winter. Additional experiments with 5 °C as low temperature level would be promising, albeit requiring a different heat sink in the laboratory. As the low heat sink temperature was the main incentive to go for a charge boost application in winter, comparably better results are expected for a low temperature level of 5 °C.

9 Conclusion

In this Master's thesis it was investigated whether the charge boost technology can be used to improve the efficiency of sorption thermal energy storage systems. Experiments have been conducted in order to provide proof of principle concerning the theoretical predictions. The results indicate that the charge boost process does indeed function as expected. This validation opens the door for a variety of applications.

In summer, this technology can be used to further charge a main storage unit which has already reached its maximum state of charge by pure desorption. By exploiting the fact that this technology can operate at a very low temperature level it can also be used in winter. The concept developed by the author suggests the use of the charge boost technology to recharge an already discharged main storage unit in winter. Being able to use low temperature heat, the charge boost technology also allows the solar thermal collectors to operate at a lower temperature level which in return increases their efficiency. The theoretical calculations show that with the charge boost technology it is even possible to match, if not exceed, the short term storage capabilities of a hot water storage tank in winter.

Generally speaking, closed sorption energy storage systems are too expensive for the market at the moment. This is due to two main reasons. Firstly, the sorption material is only produced on a small scale and therefore comparably expensive. In combination with the high demand of sorption material for a seasonal storage system by using pure desorption, this results in a high cost for just the material. This problem could be resolved by mass production of the respective materials. However, this would require an already existing market for the product in order to get the industry to invest in such processes. The second reason for the high cost of closed sorption energy storage systems is very similar to the first one and concerns the cost of vacuum components. Also the solution remains the same, with mass production as a measure to reduce the cost.

The charge boost technology is an important step in the process of getting sorption thermal energy storage systems market-ready. It tackles the problem of space uptake and material requirement by increasing the maximum possible energy storage density of the system. Furthermore, it increases the number of conducted cycles which in return decreases the specific cost of energy per mass unit storage material. In conclusion it can be stated that the charge boost technology is a viable option for the improvement of sorption thermal energy storages and a promising candidate for further research projects.

10 Appendix

10.1 Material Data

Table 10-1: Material data for all investigated adsorbents, provided by Kohl [35].

Material	E [J/g]	n [-]	W_0 [m³/kg]	Q_{ads} [Wh/kg]
Silica Gel Fuji Type 3A	217,01	1,59	0,000365	231
Silica Gel Fuji Type RD	205,85	1,40	0,000386	263
Silica Gel Sorbead R	235,17	1,51	0,000420	240
Silica Gel Sylobead SGB 127	214,12	1,33	0,000364	239
Zeolith 13XBF	1152,91	1,52	0,000333	308
AQSOA Z02	398,42	2,82	0,000307	230

Table 10-2: Parameters for the chosen collectors for the definition of the system properties [33], [34].

ref. collector	η_0 [$-$]	a_1 [W/m^{2}K]	a_2 [W/m^{2}K^2]	c_{p_coll} [J/m^{2}K]
evacuated tube	0,773	1,09	0,0094	44400

10.2 Bibliography

[1] I. Capellan-Perez and e. al., "Fossil fuel depletion and socio-economic scenarios: An integrated approach," Energy, pp. 641-666, 2014.

[2] S. Mohr and e. al., "Projection of world fossil fuels by country," Fuel, pp. 120-135, 2015.

[3] I. Dincer and C. Zamfirescu, "Fossil fuels and alternatives," in Advanced Power Generation Systems, Elsevier, 2014, pp. 95-141.

[4] N. Apergis and J. E. Payne, "Renewable energy, output, CO2 emissions, and fossil fuel prices in Central Amberca: Evidence from a nonlinear panel smooth transition vector error correction model," Energy Economics, pp. 226-232, 2014.

[5] M. Höök and X. Tang, "Depletion of fossil fuels and anthropogenic climate change - A review," Energy Policy, pp. 797-809, 2013.

[6] Z. Liu, "A Global Energy Outlook," in Global Energy Interconnection, Elsevier, 2015, pp. 91-100.

[7] T. Tereshchenko and N. Nord, "Energy planning of district heating for future building stock based on renewable energies and increasing supply flexibility," Energy, pp. 1227-1244, 2016.

[8] L. Röpke, "The development of renewable energies and supply security," Energy policy, pp. 1011-1021, 2013.

[9] C. Rohringer and R. Werner, Diplomandenseminar bei AEE Intec, Gleisdorf Österreich: AEE Intec, 2016.

[10] E. Ampatzi, I. Knight and R. Wiltshire, "The potential contribution of solar thermal collection and storage systems to meeting the energy requirements of North European Housing," Solar Energy, pp. 402-421, 2013.

[11] M. Aneke and M. Wang, "Energy storage technologies and real life applications - A state of the art review," Applied Energy, pp. 350-377, 2016.

[12] A. Hauer, S. Hiebler and M. Reuß, Wärmespeicher, Stuttgart: Fraunhofer IRB Verlag.

[13] A. Hauer, Beurteilung fester Adsrobentien in offenen Sorptionsystemen für energetische Anwendungen, Berling, 2002.

[14] I. Langmuir, "Surface chemistry," in Nobel Lecture, 1932.

[15] M. Polanyi, Theories of the adsorption of gases. A general survey and some additional remarks, 1931.

[16] W. V. Dingenen, Prüfung der Adsorptionstheorie von Polanyi durch Adsorptionsmessungen mit verschiedenen Gasen an Glas und Holzkohle unterhalb der kritischen Temperatur, Leuven, Belgien, 1939.

[17] B. P. Bering, M. M. Dubinin and V. V. Serpinsky, Theory of volume filling for vapor adsorption, Moscow: Institute of Physical Chemistry, USSR Academy of Sciences, 1965.

[18] B. P. Bering, M. M. Dubinin and V. V. Serpinsky, On the thermodynamics of adsorption in micropores, Moscow: Institute of Physical Chemistry, Academy of Sciences of the USSR, 1971.

[19] M. M. Dubinin and H. F. Stoekli, Homogeneous and heterogeneous microporestrucutres in carbonaceous adsorbents, Moscow: Institute of Physical Chemistry of the USSR Academy of Sciences, 1980.

[20] N. D. Hutson and R. T. Yang, Theoretical Basis for the Dubinin-Radushkevitch (D-R) Adsorption Isotherm Equation, Michigan: Departement of Chemical Engineering, University of Michigan, 1996.

[21] C. Nguyen and D. D. Do, "The Dubinin-Radushkevich equation and the underlying microscopic adsorption description," Department of chemical Engineering, The University of Queensland, Queensland, Australia, 2000.

[22] T. S. Jakubov and D. E. Mainwaring, "Modified Dubinin-Radushkevich/Dubinin-Astakhov Adsorption Equations," Journal of Colloid and Interface Science, pp. 263-268, July 2002.

[23] G. W. Thomson, "The Antoine Equation for Vapor-pressure Data," Chem. Rev., pp. 1-39, 1946.

[24] "www.comtes-storage.eu," [Online]. [Accessed 14 09 2016].

[25] R. Köll and e. al., "Demonstration eines saisonalen Soprtionsspeichersystems im realen Maßstab," Symposium Thermische Speicher, OTTI Neumarkt Deutschland, 2016.

[26] Y. Aristov, M. Tokarev and V. Sharonov, "Universal relation between the boundary temperatures of basic cycle of sorption heat machines," Elsevier, pp. 2907-2912, 2008.

[27] A. Hauer and E. Lävemann, Möglichkeiten offener Sorptionsspeicher zum Heizen, Klimatisieren und Entfeuchten, Garching, Deutschland: Bayrisches Zentrum für angewandte Energieforschung, ZAE Bayern.

[28] N. Khartchenko, Thermische Solaranlagen, Berlin: VWF Berlin, 1995.

[29] B. Mette, H. Kerskes, H. Drück and H. Müller-Steinhagen, "New highly efficient regeneration process for thermochemical energy storage," Applied Energy, pp. 352-359, 2013.

[30] B. Müller, Integrierter Sorptionsspeicherkollektor, Graz: Technische Universität Ilmenau, 2015.

[31] S. A. Kalogirou, "Solar thermal collectors and applications," progress in energy and combustion science, pp. 231-295, February 2004.

[32] R. Werner, Masterarbeit: Duales Ladekonzept für saisonale Sorptionswärmespeicher, Gleisdorf, 2016.

[33] W. Streicher and H. Richard, "Structure of the reference buildings of task 26," IEA SHC, 2003.

[34] R. Heimrath and M. Haller, "The reference heating system, the template solar system of task 32," IEA SHC, 2007.

[35] B. Kohl, "Short report materials," AEE Intec, Gleisdorf, 2016.

[36] W. Van Helden, "How to compare the performance of compact long term thermal energy storages," in Gleisdorf Solar, Gleisdorf, Österreich, 2016.

10.3 List of figures

10.4 List of tables